ABSTRACT

Title of Thesis : Artificial dielectric polymeric optical waveguides

Peng Chen, Master of Science, 1991

Thesis directed by : Dr. Haim Grebel

Optical Waveguide Laboratory

Wave propagation in artificial dielectric polymeric optical thin film waveguides is studied. These artificial dielectric films are made of multiple layers either metallic or semiconductor clusters in polymeric matrix. The waveguides are fabricated using the plasma polymerization and vacuumm evaporation deposition method. By analyzing results of these kinds of structures, some important conclusions can be obtained. The artificial dielectric layer in the waveguide center effectively changes the modal distribution in the waveguides. In the case of semiconductor layer, an all optical switch may be realized.

ARTIFICIAL DIELECTRIC POLYMERIC OPTICAL WAVEGUIDES

by

Peng Chen

Thesis submitted to the Faculty of the Graduate School
of New Jersey Institute of Technology
in partial fulfillment of the requirements
of the degree of Master of Science
in Electrical Engineering
1991

APPROVAL SHEET

Title of Thesis : Artificial Dielectric Polymeric Optical Waveguides

Name of Candidate : Peng Chen

Master of Science in Electrical Engineering, 1991

Thesis and Abstract Approved:

_____   _____
Dr. Haim Grebel   Date
Professor of E.E. Department

_____   _____
Dr. Edip Niver   Date
Professor of E.E. Department

_____   _____
Dr. Marek Sosnowski   Date
Professor of E.E. Department

VITA

Name : Peng Chen

Permanent address :

Degree and date to be conferred : M.S.E.E., 1991.

Date of birth :

Place of birth :

College education : Beijing University, B.S. in Physics, 1987.

Secondary education : Henan University High School.

Employment :   Optical Engineer, September 1990 — Present.
Engineered Materials Research Center,
Allied Signal Inc., Morristown, NJ.

Research Assistant, September 1988 — August 1990.
Optical Waveguide Laboratory, Dept. of E.E ,
New Jersey Institute of Technology, Newark, NJ.

Research Associate, July 1987 — August 1988.
Modern Physics Laboratory, Dept. of Physics,
Henan University, Kaifeng, P. R. China.

ACKNOWLEDGEMENTS

CONTENTS

CHAPTER 1   INTRODUCTION

The transmission and processing of signals carried by optical beams rather than by electrical currents or radio waves has been a topic of great interest ever since the early 1960's, when the development of the laser first provided a stable source of coherent light for such applications. Laser beams can be transmitted through the air, but atmospheric variations cause undesirable changes in the optical characteristics of the path from day to day, and even from instant to instant. Laser beams also can be manipulated for signal processing, but that requires optical components such as prisms, lenses, mirrors, electro-optic modulators and detectors. All of this equipment would typically occupy a laboratory bench tens of feet on a side, which must be suspended on a vibration-proof mount. Such a system is tolerable for laboratory experiments, but is not very useful in practical applications. Thus, in the late 1960's, the concept of "integrated optics" emerged, in which wires and radio links are replaced by light-waveguiding optical fibers rather than by through-the-air optical paths, and conventional electrical integrated circuits are replaced by miniaturized optical integrated circuits (OIC's). [1][2][3][4]

There are a number of advantages in optical integrated circuits, [5] such as low loss coupling, low power consumption, higher reliability, high speed and large information capacity, compared with

similar electrical integrated circuits. However, those superior performances are limited mainly by the relatively high cost to develop these technologies.

The choice of a material to fabricate an optical integrated circuit depends strongly on the function to be performed by the circuit. In most cases, the optical integrated circuit may consist of a number of different optical devices such as source, modulator, and detectors, and no one material will be optimal for all of them. So far inorganic, mainly semiconductor materials, have been studied thoroughly, for electro-optic effects.

Low-loss optical waveguides are generally fabricated from materials that may be regarded as perfect lossless dielectrics at optical frequencies. On the other hand, low-loss radio-frequency transmission lines and microwave waveguides are generally made with metal wires, strips, or tubes that may be regarded as perfect conductors at low frequencies. The reason is that the proximity of infrared lattice vibrational resonances makes it difficult to approach a perfect dielectric at low frequencies, while the proximity of the ultraviolet electron plasma resonance makes it difficult to approach a perfect conductor at optical frequencies.[6] Nevertheless, metal clad optical waveguides are of interest for certain electrolytic devices in which radio-frequency fields must be applied to a dielectric medium carrying a guided optical wave.

In this thesis, we are reporting experimental results of polymeric (PMMA, Methyl Methacrylate) waveguides with either a metallic or a semiconductor artificial dielectrics layer. The theory

of the waveguides is given by solving Maxwell's equations.

Thin film dielectric waveguides are desirable in many applications since they can be deposited conformably on various substrate, and the fabrication process is quite reliable. Several different techniques have been developed to deposit polymer films on amorphous substrates. In the solution deposit techniques, the substrate is covered with a liquid such as photoresist, polyurethane, or mixtures of two polymer solutions such as polymethyl methacrylate (PMMA) and styrene acrylonitrile copolymer (SAN). The liquid layer thickness is controlled by either spinning the substrate at a rate of several thousand rpm in an axis perpendicular to its surface, vertically dipping the substrate into the liquid and removing it at a controlled rate, or covering the substrate with liquid and subsequently turning it upright to allow excess liquid to run off. Depending upon the polymer used, the films are subsequently air dried and baked at temperatures ranging from 60 to 100°C for times varying between 5 minutes to 70 hours. The solution-deposit technique offers several potential advantages including simplicity of fabrication and required equipment, low cost, and low optical attenuation (0.1-0.3 dB/cm). However, it is difficult to control film uniformity and thickness. The second method for the deposition of polymer films involves a plasma polymerization process. In plasma polymerization, an electrical discharge is created in a vapor containing low-weight organic molecules called monomers. The discharge causes an ionization and fragmentation of the monomers and a subsequent rebonding of the fragments into a much larger two- or three-dimensional structure by a

process called polymerization. When a substrate such as glass is introduced into the discharge, the polymer is deposited on its surface. Because the resulting polymer film has many chemical bonds, it is inert to most organic solvents, mild acids, and bases and exhibits good temperature stability.[7][8] In this thesis we used the second method. Details of the fabrication equipment and process are given in Chapter 3.

There are some papers concerned with the topic of thin dielectric films with metal cladding. For example, in Kaminow's paper,[6] the properties of several planar metal-clad waveguides have been computed by using handbook values for the complex dielectric constants of the metals. However, complex dielectric constants are used throughout the paper and the thickness d is on the order of a micrometer. In this thesis, real dielectric constants are chosen to make a good understanding of physical meaning, and the waveguide structure is APMPG (Air/Polymer/Metal/Polymer/Glass) with the thickness of metal layer on the order of 10 nm.

In this thesis, multiple structure polymer waveguides are considered. These artificial dielectric films are made of layers of polymer with either metallic clusters or semiconductor clusters. By analyzing results of these kinds of structures. some important conclusions can be obtained. The artificial dielectric layer in the waveguide center effectively changes the modal distribution in the waveguide. In the case of semiconductor layer, an all optical switch may be realized.[9][10]

The theoretical analysis is given in Chapter 2. The fabrication

system and experimental procedures are explained separately in Chapter 3 and Chapter 4. Chapter 5, Chapter 6 and Chapter 7 give the experimental results and conclusions.

Chapter 2   Theory Research

2.1 Basic Theory of Slab Waveguides:

The simplest optical waveguide is the slab waveguide which consists of a film of refractive index n_2 and thickness t sandwiched between thick layers of refractive indices n_1 and n_3 (see Figure 2.1).
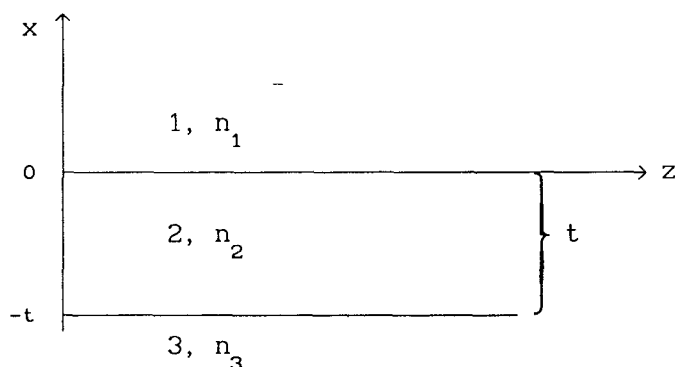
Figure 2.1   Slab waveguide structure

We will choose a coordinate system in which the film lies in the y-z plane with the slab confined between x = -t and x = 0. The symmetry of the problem allows us to ignore the y-dimension and consider propagation of light only in the x-z plane. We further will consider $n_2 > n_1$ and $n_2 > n_3$ for asymmetric case. The propagation of light is described by solutions of Maxwell's equations. These solutions show that propagation of light in the medium of Figure 2.1 under the above assumptions may be described in terms of "Guided

Modes", that is, modes in which energy is more or less confined to the region -t < x < 0 and "Radiation Modes"; that is, modes which appear to "radiate" from the 1,2 or 2,3 interfaces.

Although a quantitative description of wave propagation in slab waveguides is most easily obtained by solutions of Maxwell's equations, considerable insight into the nature of guided modes and radiation modes may be obtained from considerations of simple geometrical optics. Several physically satisfying accounts of the geometrical approach to light propagation in waveguides may be found in the literature.[8][11]-[14] Consider, for example, radiation in region 2 incident upon the 1,2 or the 2,3 interface at angle θ_2 (measured from the normal)(see Figure 2.2).
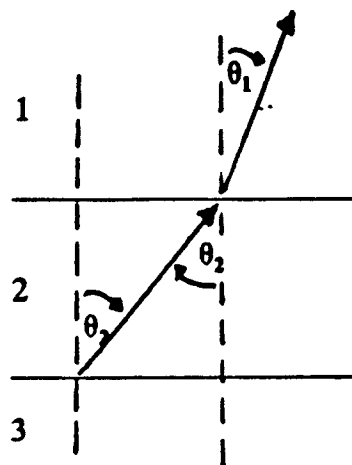
Figure 2.2   Light transmission configuration

Snell's Law[15] then gives the refracted angle for transmission

through the 1,2 interface:

$$n_2 Sin\theta_2 = n_1 Sin\theta_1 \qquad (2\text{-}1)$$

The refracted angle is thus,

$$\theta_1 = Sin^{-1}(n_2 Sin\theta_2 / n_1) \qquad (2\text{-}2)$$

It is important to note that Eq. (2-2) has no solution for $(n_2 Sin\theta_2 /$ $n_1) > 1$. In geometrical optics, this may be described the phenomenon of <u>Total Internal Reflection</u>: instead of refraction, the wave is totally reflected. Thus for angles θ_2 which exceed θ_{TIR} defined by

$$\theta_{TIR} = Sin^{-1} (n_1 / n_2). \qquad (2\text{-}3)$$

total internal reflection occurs. Figure 2.3 shows θ_{TIR} as a function of the deviation of the index ratio from 1, $[(n_2 / n_1) - 1]$:
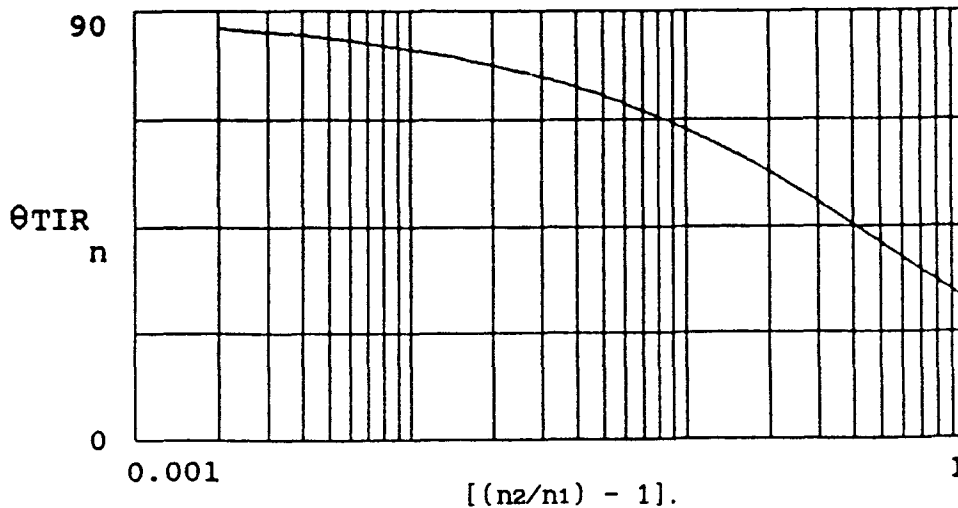
Figure 2.3 θ_{TIR} as a function of the deviation of the index ratio from 1, $[(n_2/n_1) - 1]$.

When n_2 / n_1 is within a few percent of unity, θ_{TIR} approaches $90°$; that is, only for near grazing incidence does total internal reflection take place. We may thus note that when θ_2 is less than the critical angle, total internal reflection does not take place and the wave of Figure 2.2 radiates. When incident angles at both interfaces are greater than the critical angle, then total internal reflection occurs at both interfaces, and the beam is confined (or guided) by the interfaces:
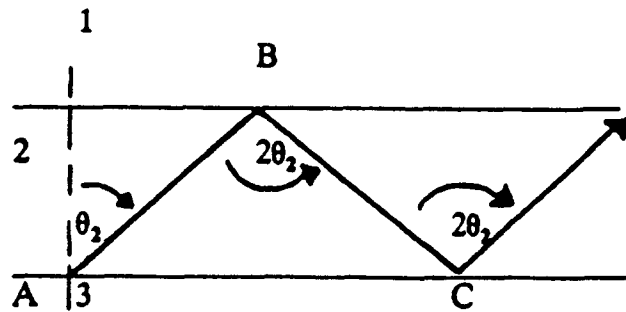
Figure 2.4   Total internal reflection phenomenon.

Thus the phenomenon of guided waves can occur only if $n_2 > n_1$, n_3 and if θ_2 exceeds the largest of the critical angles θ_{TIR} for the 1,2 and 2,3 interfaces.

2.2 Waveguide Configurations:

The waveguide structures with metallic and semiconducting artificial dielectrics are shown schematically in Figure 2.5 and Figure 2.6 respectively. The transverse mode is subject to three conditions at the interfaces: the air-polymer, the polymer-artificial dielectric and the polymer-glass substrate interfaces.

AIR

```
+-------------------------------------+
|                                     |
|              POLYMER                |
|                                     |
+-------------------------------------+  ⌐Al
|                                     |
|              POLYMER                |
|                                     |
+-------------------------------------+
```

GLASS SUBSTRATE

Figure 2.5 Waveguide Configuration

AIR

```
+-------------------------------------+
|                                     |
|              POLYMER                |
|                                     |
+-------------------------------------+  ⌐CdS
|                                     |
|              POLYMER                |
|                                     |
+-------------------------------------+
```

GLASS SUBSTRATE

Figure 2.6 Waveguide Configuration

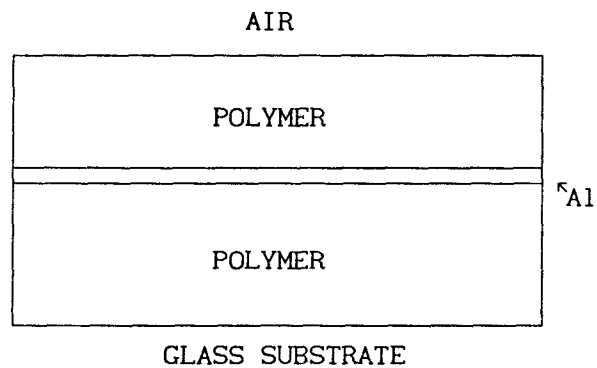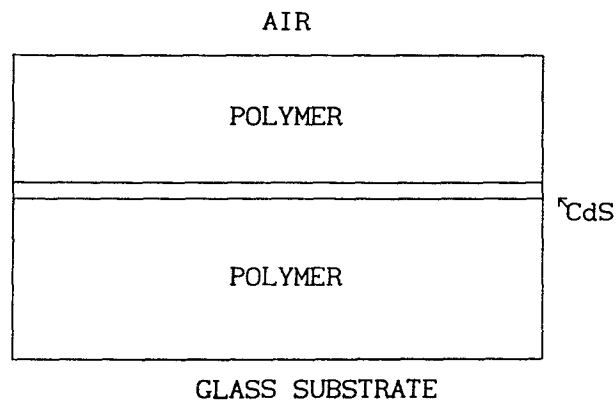As mentioned above, the propagation of light is described by solutions of Maxwell's equations. In section 2.4 and 2.5 the method to get graphical eigenvalue solutions of three-layer structure waveguides by using computer programs is discussed. During solving procedures, the TE (Transverse Electric) mode and TM (Transverse Magnetic) mode are both considered in the same method by assuming different boundary conditions. The eigenvalue equations are derived by solving Maxwell's equations. The graphical solutions, the eigenvalues, electrical field distributions and intensity distributions of different modes can be obtained by using these computer programs.

2.3 Maxwell's Equations and Boundary Conditions:

In a medium of magnetization density M and polarization density P, Maxwell's equations in mks units for the electric field E (V/m), and the magnetic field (intensity) H (A/m) are:

Faraday's law:

$$\nabla \times E = - \frac{\partial}{\partial t} \mu_0 H - \frac{\partial}{\partial t} \mu_0 M \qquad (2-4)$$

Ampere's law:

$$\nabla \times H = \frac{\partial}{\partial t} \varepsilon_0 E + \frac{\partial P}{\partial t} + J \qquad (2-5)$$

Gauss's law for the electric field:

$$\nabla \cdot \varepsilon_0 E = - \nabla \cdot P + \rho \qquad (2-6)$$

Gauss's law for the magnetic field:

$$\nabla \cdot \mu_0 H = - \nabla \cdot \mu_0 M \qquad (2-7)$$

where ρ is the charge density and J is the current density produced by

all charges other than those associate with polarization. The constants in Maxwell's equations are:

$$\varepsilon_0 \cong \frac{1}{36\pi} \times 10^{-9} \ \frac{A \cdot s}{V \cdot m}$$

the dielectric constant of free space, and

$$\mu_0 = 4\pi \times 10^{-7} \ \frac{V \cdot s}{A \cdot m}$$

the magnetic permeability of free space.

If the medium is linear, isotropic and dispersion-free. Then Maxwell's equations can be rewritten as:

$$\nabla \times E = \mu \frac{\partial H}{\partial t} \qquad\qquad (2\text{-}8)$$

$$\nabla \times H = \varepsilon \frac{\partial E}{\partial t} + J \qquad\qquad (2\text{-}9)$$

$$\nabla \cdot \varepsilon E = \rho \qquad\qquad (2\text{-}10)$$

$$\nabla \cdot \mu H = 0 \qquad\qquad (2\text{-}11)$$

Consider a source free medium, $\rho = J = 0$. The wave equation (2-12) can be derived from Maxwell's equations:

$$\nabla^2 E = \mu\varepsilon \frac{\partial^2 E}{\partial t^2} \qquad\qquad (2\text{-}12)$$

when ε is uniform and $\nabla \cdot E = 0$.

Boundary Conditions:

(1) Normal component of B is continuous.

$$n \cdot (B_2 - B_1) = 0 \qquad\qquad (2\text{-}13)$$

(2) Tangential component of E is continuous.

$$n \times (E_2 - E_1) = 0 \qquad\qquad (2\text{-}14)$$

(3) Normal component of D is discontinues by the amount of the surface charge density.

$$n \cdot (D_2 - D_1) = \rho_s \qquad\qquad (2\text{-}15)$$

(4) Tangential component of H is discontinues by the amount of the

electric surface charge density.

$$\mathbf{n} \times (\mathbf{H_2} - \mathbf{H_1}) = j_s \tag{2-16}$$

In case of source-free simple matter (linear, isotropic and homogeneous), Eq. (2-15) and (2-16) can be written as:

$$\mathbf{n} \cdot (\mathbf{D_2} - \mathbf{D_1}) = 0 \tag{2-17}$$

$$\mathbf{n} \times (\mathbf{H_2} - \mathbf{H_1}) = 0 \tag{2-18}$$

2.4 TE (Transverse Electric) Mode:

Assume time variant is $e^{j(\omega t - \beta z)}$.

The sample structure, shown in Figure 2.7 is divided into 5 layers:

(1) Air, $n_a = 1.00$, $\mu = \mu_o$. $a+b+t < x < +\infty$.

(2) PMMA layer, $n_p = 1.50$, $\mu = \mu_o$. $a+t < x < a+b+t$.

(3) Aluminum layer, $n_{Al} = 1.52$, $\mu = \mu_o$. $a < x < a+t$.

(4) PMMA layer, same as (2). $0 < x < a$.

(5) Glass substrate, $n_g = 1.498$, $\mu = \mu_o$. $-\infty < x < 0$.
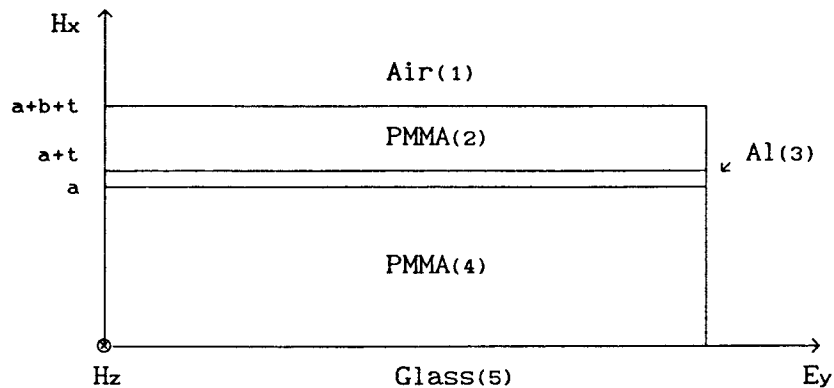

Figure 2.7   Waveguide sample structure

The E-field in different layers should be:

(1) $E_y = A\ e^{-\gamma_a x}$ $a+b+t < x < +\infty.$

(2) $E_y = B\ \cos k_x x + B'\sin k_x x$ $a+t < x < a+b+t.$

(3) $E_y = C\ \cos k_x' x + C'\sin k_x' x$ $a < x < a+t.$

(4) $E_y = D\ \cos k_x x + D\sin k_x x$ $0 < x < a.$

(5) $E_y = E\ e^{\gamma_g x}$ $-\infty < x < 0.$

Associate H-fields:

$$\begin{cases} H_x = -\ (\dfrac{j}{\omega\mu_0})\dfrac{\partial E_y}{\partial z} \\[2mm] H_z = (\dfrac{j}{\omega\mu_0})\dfrac{\partial E_y}{\partial x} \end{cases}$$

(1) $H_z = \dfrac{-jA\gamma_a}{\omega\mu_0}\ e^{-\gamma_a x}$ $a+b+t < x < +\infty.$

(2) $H_z = \dfrac{jk_x}{\omega\mu_0}\ [-B\ \sin k_x x + B'\cos k_x x\ ]$ $a+t < x < a+b+t.$

(3) $H_z = \dfrac{jk_x'}{\omega\mu_0}[-C\ \sin k_x' x + C'\cos k_x' x\ ]$ $a < x < a+t.$

(4) $H_z = \dfrac{jk_x}{\omega\mu_0}[-D\ \sin k_x x + D'\cos k_x x\ ]$ $0 < x < a.$

(5) $H_z = \dfrac{jE\gamma_g}{\omega\mu_0}\ e^{\gamma_g x}$ $-\infty < x < 0.$

We ignore H_x-component for small value compared to other field components.

Using the boundary condition Eq. (2-14):

At $x = a+b+t$:

$A\ e^{-\gamma_a(a+b+t)} = B\ \cos k_x(a+b+t) + B'\sin k_x(a+b+t)$ (1)

At $x = a+t$:

$$B \cos k_x(a+t) + B'\sin k_x(a+t) = C \cos k_{x'}(a+t) + C'\sin k_{x'}(a+t) \qquad (2)$$

At $x = a$:

$$C \cos k_{x'}a + C'\sin k_{x'}a = D \cos k_x a + D'\sin k_x a \qquad (3)$$

At $x = 0$:

$$D = E \qquad (4)$$

Using the boundary condition Eq. (2-13):

For simple matter, $\overline{B} = \mu \overline{H}$.

At $x = a+b+t$:

$$-A \gamma_a e^{-\gamma_a(a+b+t)} = k_x [-B \sin k_x(a+b+t) + B'\cos k_x(a+b+t)] \qquad (5)$$

At $x = a+t$:

$$k_x[-B \sin k_x(a+t)+B'\cos k_x(a+t)]=k_{x'}[-C \sin k_{x'}(a+t)+C'\cos k_{x'}(a+t)] \qquad (6)$$

At $x = a$:

$$k_{x'}[-C \sin k_{x'}a + C'\cos k_{x'}a] = k_x[-D \sin k_x a + D'\cos k_x a] \qquad (7)$$

At $x = 0$:

$$k_x D' = \gamma_g E \qquad (8)$$

From Eq.(4) & (8):

$$\frac{D'}{D} = \frac{\gamma_g}{k_x} \qquad (a)$$

From Eq.(1) & (5):

$$-\gamma_a = k_x \left[\frac{-B \sin k_x(a+b+t) + B'\cos k_x(a+b+t)}{B \cos k_x(a+b+t) + B'\sin k_x(a+b+t)} \right]$$

or,

$$\frac{B'}{B} = \frac{\tan k_x(a+b+t) - (\gamma_a/k_x)}{1 + (\gamma_a/k_x)\tan k_x(a+b+t)} \qquad (b)$$

From Eq.(3) & (7):

$$k_x' \left[\frac{-C \sin k_x'a + C' \cos k_x'a}{C \cos k_x'a + C' \sin k_x'a} \right] = k_x \left[\frac{-D \sin k_x a + D' \cos k_x a}{D \cos k_x a + D' \sin k_x a} \right]$$

Put (a) into above equation, we can get:

$$\frac{C'}{C} = \frac{-k_x^2 \tan k_x a + \gamma_g k_x + k_x k_x' \tan k_x' a + \gamma_g k_x' \tan k_x a \cdot \tan k_x' a}{k_x k_x' + \gamma_g k_x \tan k_x a - \gamma_g k_x \tan k_x' a + k_x^2 \tan k_x a \cdot \tan k_x' a} \quad (c)$$

From Eq.(2) & (5):

$$k_x \left[\frac{-B \sin k_x(a+t) + B' \cos k_x(a+b)}{B \cos k_x(a+t) + B' \sin k_x(a+t)} \right] = k_x' \left[\frac{-C \sin k_x'(a+t) + C' \cos k_x'(a+t)}{C \cos k_x'(a+t) + C' \sin k_x'(a+b)} \right]$$

or,

$$\frac{-\tan k_x(a+t) + (B'/B)}{1 + (B'/B)\tan k_x(a+t)} = \frac{k_x'}{k_x} \left[\frac{-\tan k_x'(a+t) + (C'/C)}{1 + (C'/C)\tan k_x'(a+t)} \right] \quad (d)$$

If a mode can propagate in the waveguide, then:

$$\gamma_a^2 = \beta^2 - n_a^2 K^2$$

$$k_x^2 = n_p^2 K^2 - \beta^2$$

$$k_x^{2'} = n_{AI}^2 K^2 - \beta^2$$

$$\gamma_g^2 = \beta^2 - n_g^2 K^2$$

so we get:

$$\gamma_a^2 = (n_p^2 - n_a^2)K^2 - k_x^2 \quad (e)$$

$$k_x^{2'} = (n_{AI}^2 - n_p^2)K^2 + k_x^2 \quad (f)$$

$$\gamma_g^2 = (n_p^2 - n_g^2)K^2 - k_x^2 \quad (g)$$

Put (b), (c), (e), (f) and (e) into (d), so we get the eigenvalue equation for TE mode. The eigenvalue equation can be solved graphically by using the computer programs which is attached in Apendix.

2.5 TM (Transverse Magnetic) Mode:

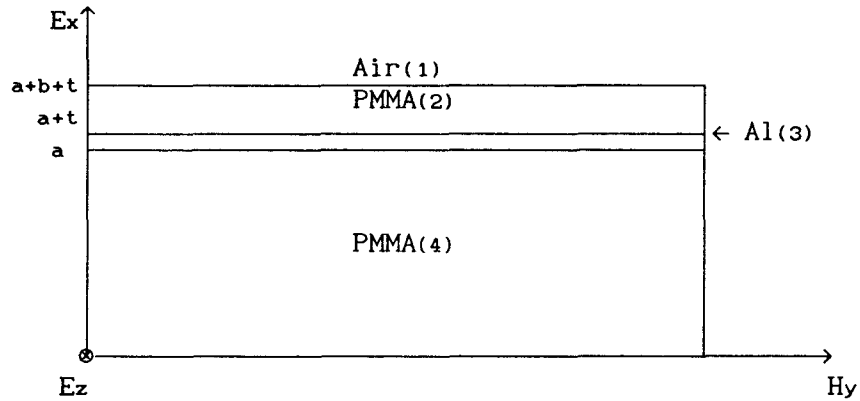Assume the time variant is $e^{j(\omega t - \beta z)}$.

Figure *2.8*   Waveguide sample structure.

As previously the sample structure is divided into 5 layers. The H-field in different layer should be:

(1) $H_y = A\ e^{-\gamma_a x}$ $a+b+t < x < +\infty.$

(2) $H_y = B\ \cos k_x x + B'\sin k_x x$ $a+t < x < a+b+t.$

(3) $H_y = C\ \cos k_x' x + C'\sin k_x' x$ $a < x < a+t.$

(4) $H_y = D\ \cos k_x' x + D'\sin k_x' x$ $0 < x < a.$

(5) $H_y = E\ e^{-\gamma_g x}$ $-\infty < x < 0.$

The associate E-fields are:

$$\begin{cases} Ex = \dfrac{j}{\omega\varepsilon} \dfrac{\partial Hy}{\partial z} \\[2em] Ez = -\dfrac{j}{\omega\varepsilon} \dfrac{\partial Hy}{\partial x} \end{cases}$$

Ez components are:

(1) $\quad Ez = \dfrac{-j}{\omega\varepsilon_o} (-A\gamma_a)\, e^{-\gamma_a x}$ $\qquad\qquad\qquad$ $a+b+t < x < +\infty.$

(2) $\quad Ez = \dfrac{-jk_x}{\omega\varepsilon_p} [-B\,\sin k_x x + B'\cos k_x x\,]$ $\qquad$ $a+t < x < a+b+t.$

(3) $\quad Ez = \dfrac{-jk_x'}{\omega\varepsilon_{Al}} [-C\,\sin k_x' x + C'\cos k_x' x\,]$ $\qquad$ $a < x < a+t.$

(4) $\quad Ez = \dfrac{-jk_x}{\omega\varepsilon_p} [-D\,\sin k_x x + D'\cos k_x x\,]$ $\qquad$ $0 < x < a.$

(5) $\quad Ez = \dfrac{-j}{\omega\varepsilon_g} E\,\gamma_g\, e^{\gamma_g x}$ $\qquad\qquad\qquad\qquad$ $-\infty < x < 0.$

Ex components are:

(1) $\quad Ex = \dfrac{1}{\omega\varepsilon_o} \beta_a\, A\, e^{-\gamma_a x}$ $\qquad\qquad\qquad$ $a+b+t < x < +\infty.$

(2) $\quad Ex = \dfrac{1}{\omega\varepsilon_p} \beta_p\, [B\,\cos k_x x + B'\sin k_x x]$ $\qquad$ $a+t < x < a+b+t.$

(3) $\quad Ex = \dfrac{1}{\omega\varepsilon_{Al}} \beta_{Al}\, [C\,\cos k_x' x + C'\sin k_x' x]$ $\qquad$ $a < x < a+t.$

(4) $\quad Ex = \dfrac{1}{\omega\varepsilon_p} \beta_p\, [D\,\cos k_x x + D'\sin k_x x]$ $\qquad$ $0 < x < a$

(5) $\quad Ex = \dfrac{1}{\omega\varepsilon_g} \beta_g\, E\, e^{\gamma_g x}$ $\qquad\qquad\qquad\qquad$ $-\infty < x < 0$

From the boundary conditions, Ez and Hy should be continuous at the boundary of different layers. So eight equations can be derived from boundary conditions.

H_y component should be continuous at the boundary:

(1) $A\ e^{-\gamma_a(a+b+t)} = B\ \cos k_x(a+b+t) + B'\sin k_x(a+b+t)$

(2) $B\ \cos k_x(a+t) + B'\sin k_x(a+t) = C\ \cos k_x'(a+t) + C'\sin k_x'(a+t)$

(3) $C\ \cos k_x'a + C'\sin k_x'a = D\ \cos k_xa + D'\sin k_xa$

(4) $D = E$

E_z component should be continuous at the boundary:

(5) $\varepsilon_p(-A\gamma_a)e^{-\gamma_a(a+b+t)} = \varepsilon_o k_x[-B\ \sin k_x(a+b+t) + B'\cos k_x(a+b+t)]$

(6) $\varepsilon_{Al} k_x[-B\ \sin k_x(a+t) + B'\cos k_x(a+t)] =$

$\varepsilon_p k_x'[-C\ \sin k_x'(a+t) + C'\cos k_x'(a+t)]$

(7) $\varepsilon_p k_x'[-C\ \sin k_x'a + C'\cos k_x'a] = \varepsilon_{Al} k_x[-D\ \sin k_xa + D'\cos k_xa]$

(8) $\varepsilon_g\ D'k_x = \varepsilon_p\ E\ \gamma_g$

Also the eigenvalue equation for TM mode can be derived from Eq.(1)-(8). The graphical method is exactly the same as that of TE mode, using the computer programs given in the Appendix.

CHAPTER 3   FABRICATION SYSTEM

3.1 System Purpose:

A fabrication system is designed to get high quality surface PMMA waveguides at relatively high generation rate.

3.2. System Configuration:

The system configuration is shown in Figure 3.1. The apparatus consists of four main parts: (1) vacuum chamber with pumping system; (2) monomer gas source with flow control valve; (3) electrodes with substrate holder; (4) ac power supply with the control timer.
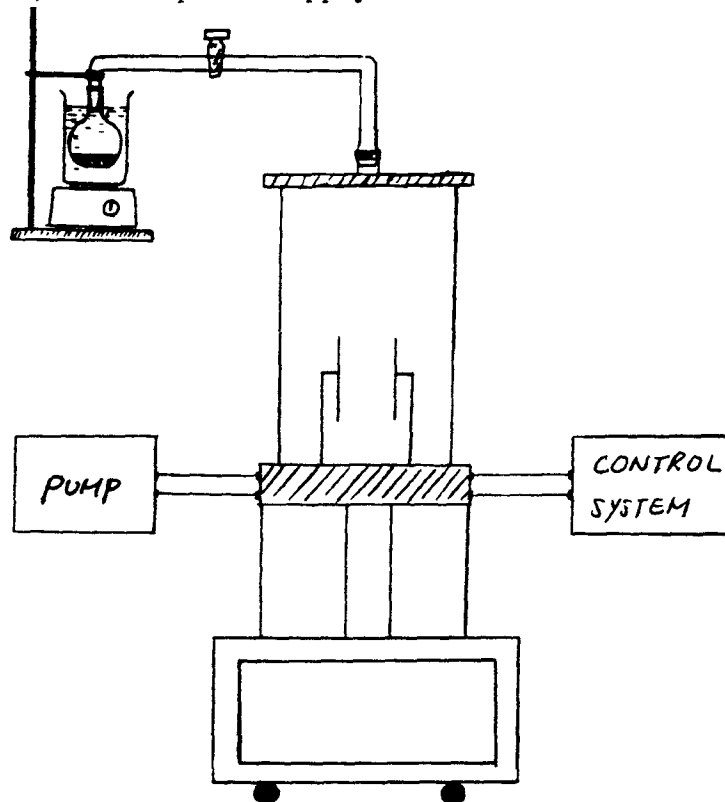

Figure 3.1   Fabrication system configuration.

3.2.1 Electrodes with the substrate holder:

The AC-induced plasma apparatus is shown in Figure. 3.2, it includes two parts: the planar brass electrodes (square in 4x4 inch^2) and a two-step transformer power system which can provides over 1000 V AC voltage. This apparatus can generate strong plasma to make the monomer ionized.
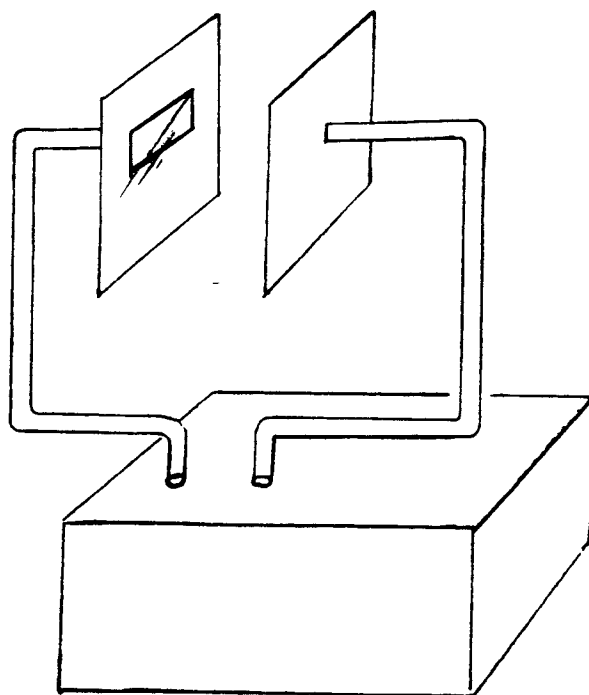

Figure 3.2 AC-induced plasma apparatus.

3.2.2 Chamber and Pump:

The chamber, of cylinderical shape 25cm in diameter and 60cm in high was used to contain the plasma apparatus. A mechanical pump is provided 1 mT vacuum measured by a thermo-couple type gauge.

3.2.3 Monomer gas source:

Figure 3.3 shows the monomer gas source. A flask is used to contain the liquid PMMA monomer and a hot plate is used to heat the flask to get higher monomer flow. Also by adjusting the valve the change on flow amount can be gained.
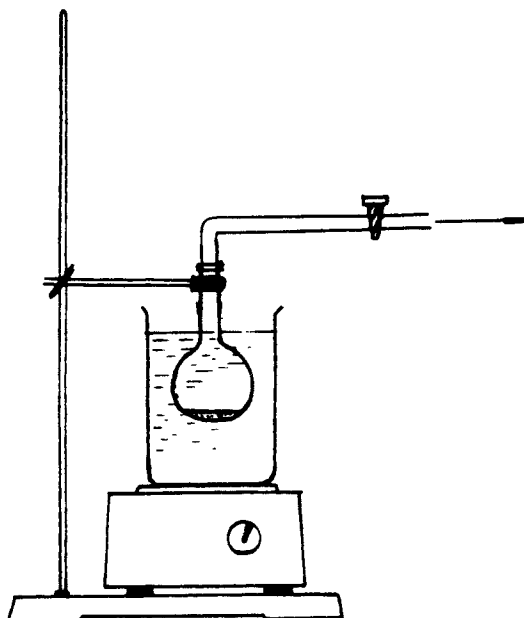

Figure 3.3   Gas flow source configuration.

3.2.4 System controller:

Figure 3.4 shows the control system configuration. This system controller is designed to control and monitor the fabrication process. By using this controller the voltage between two electrodes and the current in the circuit can be adjusted. Also the vacuum inside the chamber can be measured.
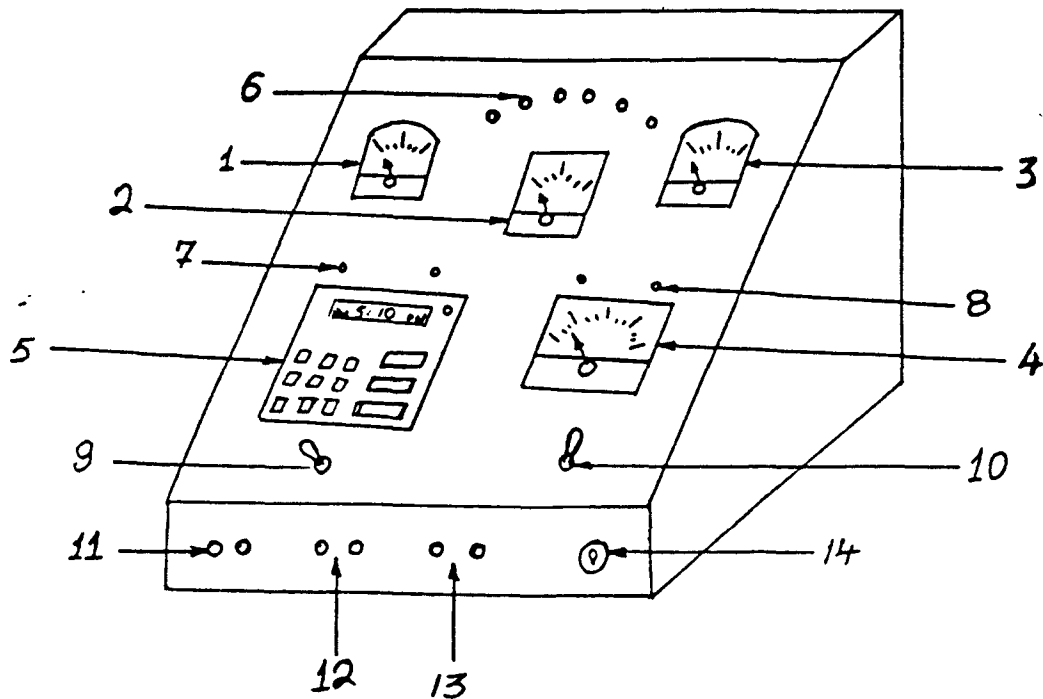
Figure 3.4   Control system configuration.

(1) DC Volt meter; (2) AC Volt meter; (3) DC Volt meter; (4) Pressure meter; (5) Button panel with LED display; (6) Green LED indicate the system is ready for operation; (7) Two LEDs, green and red; (8) Two LEDs, green and red; (9) A switch to switch the LEDs of item 7 to the desired condition; (10) A switch to switch the LEDs of item 8 to the desired condition; (11) Terminals for the output; (12) Input terminals; (13) Terminals for the vacumm pump; (14) A key to turn the whole system on.

• This part of work is done by Faisal A. Nabulsi as his Master's project.

3.3 Optimum Fabrication Condition:

Two important things, the quality of the waveguide and the generation rate have to be considered at the same time. The monomer

should be totally ionized when passing through the electrodes to get very smooth and transparent waveguide samples. In P. K. Tien's paper,[16] the generation rate is about 2000 Å/min for VTMS films and 1000 Å/min for HMDS films by coupling 200 W of RF energy from a 13.56 MHz generator to the electrodes. In our fabrication system, the optimum generation rate is about 330 Å/min. Sometimes a high quality surface can be obtained under a low generation rate, while a larger deposition speed results in a bad quality surface. From many experiments, the following optimum fabrication conditions were deduced: the vacuum inside the chamber should be 600 mT and the AC voltage between two electrodes should be 1000 V.

CHAPTER 4   EXPERIMENT

4.1 Planar Waveguides Fabrication

4.1.1 Materials Preparation:

1.   Micro-slide glass substrate.

2.   Liquid dehibited methyl methacrylate (PMMA) monomer.

3.   Methanol, acetone and distilled water.

4.1.2 Fabrication Procedures:

1. Substrate cleaning:

(1). Put the substrate (glass microscope slides 80×25×1 mm^3 with index refraction n_g=1.498 at 0.6328 μm) into a beaker which contains methanol, then put the beaker into Ultrasonic bath for 30 minutes.

(2). Wash both sides of the substrate by using acetone and distilled water.

(3). Let the substrate dry in a very clean environment.

(4). Labeled the substrate.

Now the substrate is clean and recognized.

2. PMMA-layer fabrication:

(1). Place the substrate on the electrode inside the chamber of the plasma fabrication system.

(2). Pump the system to make the vacuum smaller than 1mτ by using the

mechanical pump for 1 hour.

(3). Open the upper gate very gently to let PMMA monomer vapor flow in and change the vacuum to 600mT.

(4). Turn on and turn off the ac high voltage (1000 V) every half hour (to keep the temperature of electrode low), account time.

(5). After finishing the experiment, remove the sample out of the chamber very carefully when temperature of the system is down.

(6). Keep the sample in the stove at the temperature of 400°F for 2-3 hours.

3. Al-layer fabrication:

(1). Put the substrate into JEOL metal evaporation system, make the sample face to the source.

(2). Add proper amount of Al to the source.

(3). Close the chamber and pump vacuum of the system first by using mechanical pump smaller than 1mT, it need about 0.5 hour.

(4). By using diffusion pump for 0.5 hour, vacuum 10^{-3}mT can be gained.

(5). Turn the heat current on for 3 seconds, an 20 nm uniform Al-layer can be obtained.

4. CdS-layer fabrication:

, The CdS thin film is vapor deposited in a vacuum system. The vapor-deposition technique can produce a layer with many nucleation sites for film thickness less than 2 nm. [10]

• This part of work is done by Varsha Sheladia.

4.1.3. Thickness Control:

The measurement of coated PMMA-layer thickness can be approximated by measuring the weight increase of the micro-slide substrate by assuming the density of PMMA is 1 g/cm^3. The thickness can be also estimated from the near-field intensity distribution pattern.

In the above procedures, the thickness of waveguides can be controlled by the following:

1. Control F, which is the flow amount per unit time, the larger the factor F is, the thicker the layer is during a same period of time.

2. Control V, which is the AC voltage which induced plasma, the larger the factor V is, the thicker the layer coated.

Two important things, the generation rate and the quality of sample's surface, should be considered at the same time. It means both of them, not only one of them. From hundreds of experiments with the plasma deposition system, the maximum generation rate of 330 Å / min. was obtained (Thickness of 4 μm should take 2 hours). The vacuum inside the chamber was 600 mτ and the AC voltage V was equal to 1000 V.

4.2 TE ↔ TM Converted Measurement System

4.2.1 System Components:

1. Laser: He-Ne laser, wavelength λ=0.6328μm, output power P=1mW, beam diameter D=1mm.

2. Chopper: used with Lock-in Amplifier.

3. Lock-in Amplifier: with a reference frequency provided by chopper, to magnify the signal from the detector and to reduce the noise to minimum.

4. Half Plate: to change the polarization.

5. Objective B (x20): to focus the laser beam onto the waveguide sample. At the focal point the spot size can be calculated by using the diffraction formula of a circular aperture:[15]

$$r = 1.22 \cdot \frac{f\lambda}{D}$$

where r: radius of spot,

     λ: optical wavelength, $\lambda = 0.6328\mu m$,

     f: focal length of lens used,

     D: the diameter of laser beam.

In the experiment, the spot size is approximately $7\mu m$.

6. Waveguide Stand: to hold samples.

7. Objective A (x20): to magnify the near-field pattern of the waveguide output.

8. Detector: to detect light intensity on screen and send the signal to Lock-in Amplifier.

9. Screen: to help in observation of the waveguide phenomena.

10. Polarizer: to check the polarization state.

11. Lock-in Amplifier

In the experiment, the output signal is detected by a photo detector. A chopper which can provide a reference frequency to the Lock-in Amplifier is used to reduced the background noise to the minimum because the intensity of expected light is very weak. The

laser beam can be modulated by this chopper, in other word, the laser beam will carry "frequency information" after passes through the chopper. The total signal, which includes the background noise and expected signal, is send to the detector. By comparing the signal from the detector to the reference frequency from the chopper, the background noise which does not pass through the chopper is removed to minimum. The frequency of the chopper is chosen not to be near the frequency of the power system, 60 Hz or its integer multiplication.

4.2.2 Polarization Change by Using Half Plate:

The laser output is mainly in TE mode in respect to the waveguide axis. In our coordinate system, the light is polarized along "y" direction. By using the half plate, the state of polarization can be changed as expected. It means that we can change the light into TM mode in respect to the waveguide axis, or mainly polarized along "x" direction. There are three steps to set up the mode change:

1. Remove half plate from the measurement system.

2. Tune the polarizer to get the minimum output, then rotate 90° fromthe original place, so polarization of the polarizer is along "y" direction.

3. Put the half plate into the measurement system, rotate the halfplate until the output coming out from the polarizer is minimal. So the polarization state of the light out from the half plate is along "x" direction. Rotate the half plate by 45°, the polarization state out from the half plate is along "y" direction.

4.3 Near-field Intensity Distribution Measurement

4.3.1 Experimental Configuration:

The experimental configuration is shown in Figure 4.1. Near-field measurement of the polymeric waveguide intensity profile is made with the help of the chopper and a lock-in amplifier to increase the signal-to-noise ratio and He-Ne laser.

4.3.2 Detector:

We use the measurement system mentioned before. The laser beam passes through waveguide samples and is magnified by objective A. The magnification depends on the distance between the objective A and photo detector. Because of the very thin layer samples and near-field measurement, a pin hole is necessary in front of the photo detector. The diameter of the pin hole is around 60 μm. The pin hole is mounted together with the photo detector on a transporter which provides a x-directional scan movement. The intensity distribution can be obtained by scanning in the same interval distance.

4.3.3 Measurement Procedure:

1. Set up the measurement system.

2. Check the TE $\leftrightarrow$ TM conversion.

3. Put the sample onto waveguide stand. Adjust all 9 available tuners to get the best launching condition under both modes.

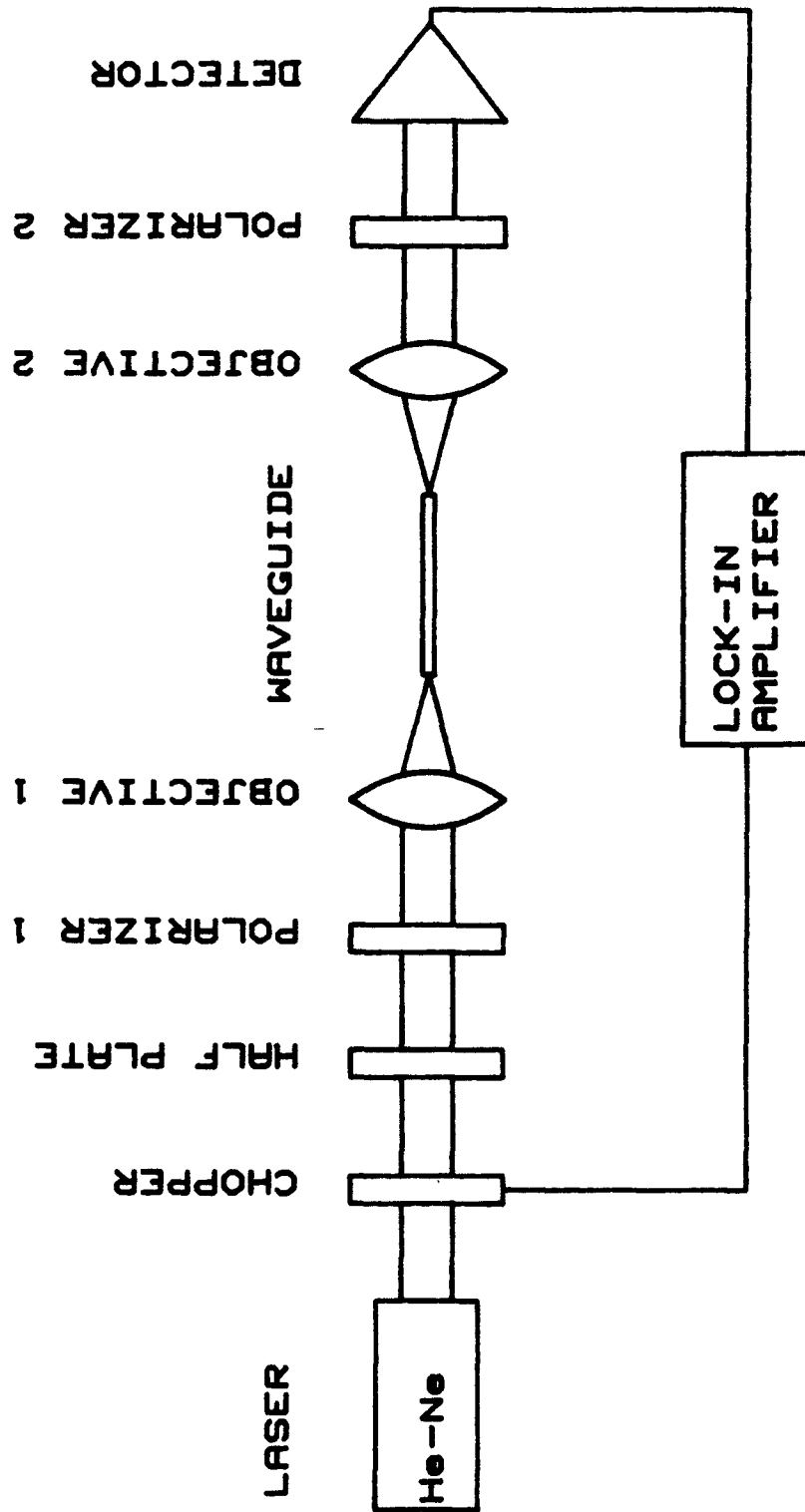4. Let the reference frequency of chopper be 210 Hz, select proper range.

31

Figure 4.1 Experimental configuration.

DETECTOR

POLARIZER 2

OBJECTIVE 2

WAVEGUIDE

OBJECTIVE 1

POLARIZER 1

HALF PLATE

CHOPPER

LASER

He-Ne

LOCK-IN
AMPLIFIER

5. Scan the total distribution before measurement. Make the reading value be zero by adjusting the phase button when the maximum value is read, then press 90° phase button.

6. From the starting point, scan every 10 μm and read the data.

7. Rotate the half plate by 45°, do the same step as 6.

8. Plot the Intensity vs Distance by using HP plotter.

4.4 Waveguide Scattering Measurement

4.4.1 Experimental Set Up:

The measurement system for near-field scattering measurment has also been setup. In this technique a set of highly focused collection optics is scanned along the length of the waveguide. Light from the He-Ne laser is coupled through an optical lens into the waveguide. The collection optics focus the light into a photodetector that measures optical power scattered from the waveguide. The resulting data can be plotted as scattered power vs waveguide length. Information about waveguide intrinsic losses, coupling losses and the distribution of scattering sites in the waveguide can be extracted directly from the plot. The photo detector is arranged above the waveguide instead of at the end of the sample. The difference is shown in Figure 4.2. The measurement procedure is almost the same as the near-fieldmeasurement except the photo detector is moved along "z" direction (waveguide length direction) and the interval distance is 1 mm.
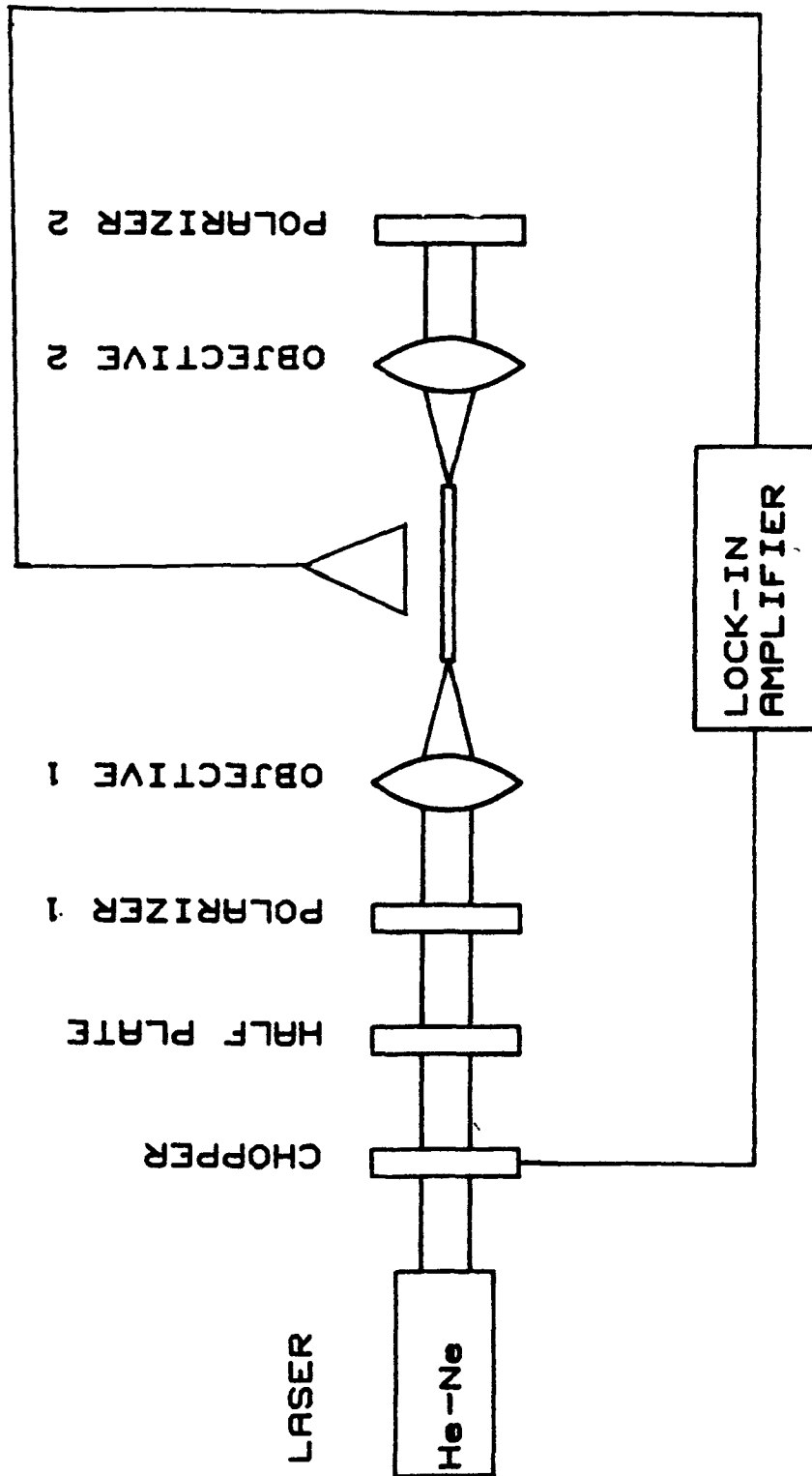
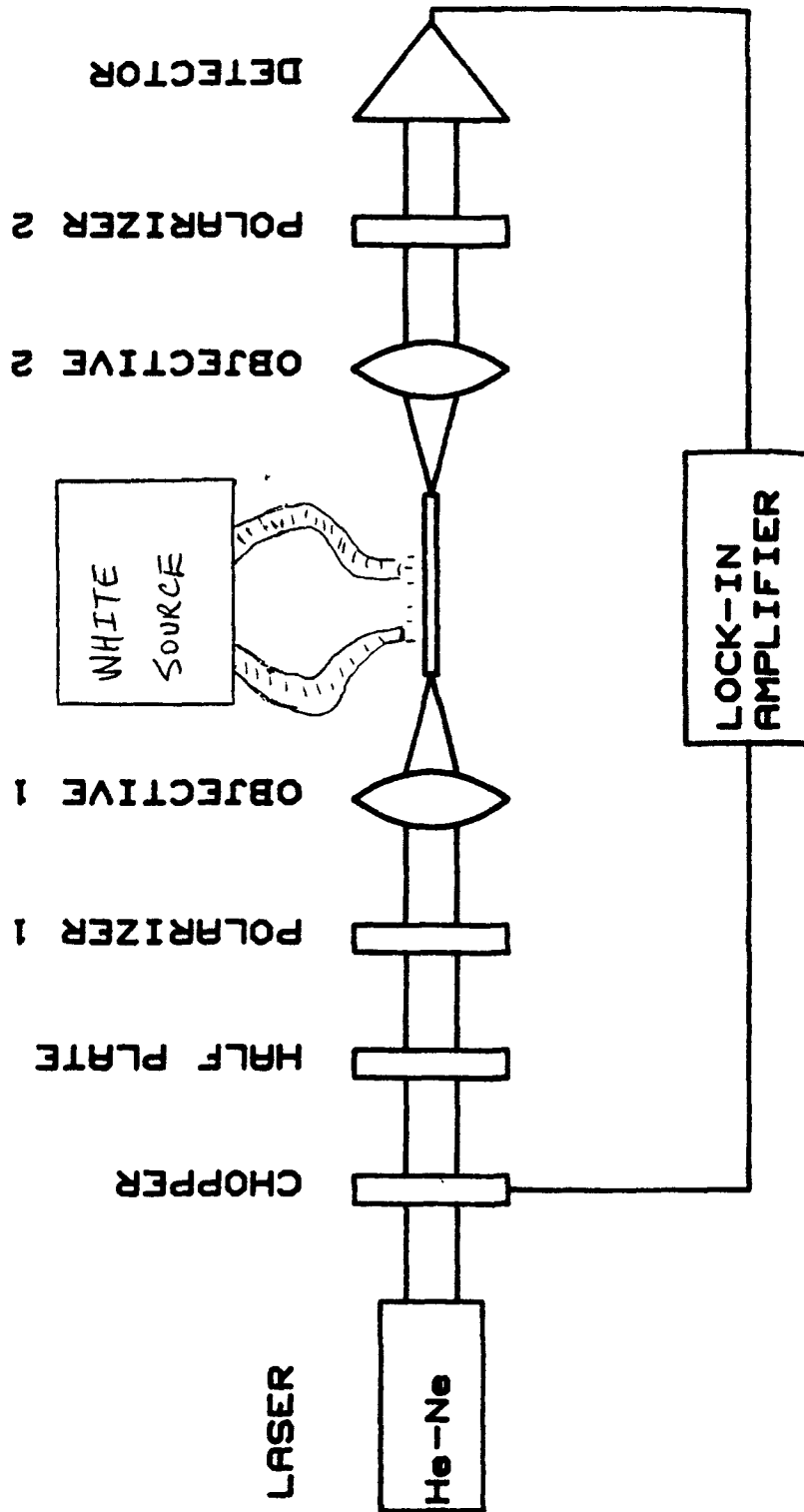*Figure 4.2* Experimental configuration for scattering measurement.

34

Figure 4.3 Experimental configuration for CdS sandwiched waveguides.

4.4.2 Scattering Measurement:

The scattering measurement is used to determine and compare the scattering factor of the different waveguides under different modes.[17] The thin Al-layer PMMA waveguide sample (thickness is around $7\mu m$) is selected to do this experiment. The experiment results and discussions will be treated in next chapter.

4.5 Intensity profiles of Semiconductor Samples:

The optical measurement system is almost the same as that in Figure 4.1 except a light source, which can submit the uniform external illumination with a strong power about 150 W, is added above the surface of the waveguide sample. Figure 4.3 shows the difference. The measurement procedures are very similar to that of metallic sandwiched samples. Near-field intensity profiles are measured before and after the light source is turned on under TE mode and TM mode. The experimental results and discussions are mentioned in the following chapter.

CHAPTER 5 ANALYSIS OF MEASUREMENTS

5.1 Field and Intensity Profiles of Metallic Sandwiched Waveguides

5.1.1 Theoretical Results:

Program 1, program 2 and program 3 (see Appendix) are devised to solve the eigenvalue equations which were derived in section 2.4 and 2.5 of Chapter 2. Figure 5.1 is the graphical solutions of TE modes for regular polymer waveguide (pure PMMA only) with these following parameters:

Total thickness T = 7.02 μm.

Index refraction of PMMA N_p = 1.50.

From Figure 5.1, there are totally two cross points of the two curves, it means there are two TE modes which can satisfy the boundary conditions, i.e., Mode TE_0 and mode TE_1 can propagate in this regular PMMA waveguide. These two cross points are enlarged separately in Figure 5.1-(1) and Figure 5.1-(2). So the eigenvalues of TE_0 and TE_1 mode can be obtained graphically (see Figure 5.1-(1) and 5.1-(2)).

The unnormalized electric field and normalized (energy is normalized to unity) intensity distributions of TE_0 mode are shown in Figure 5.2-(1) and 5.2-(2). Obviously, the tail in the glass substrate is much longer than that in air. The reason is that: at the glass substrate-polymer interface, the index refraction difference is very
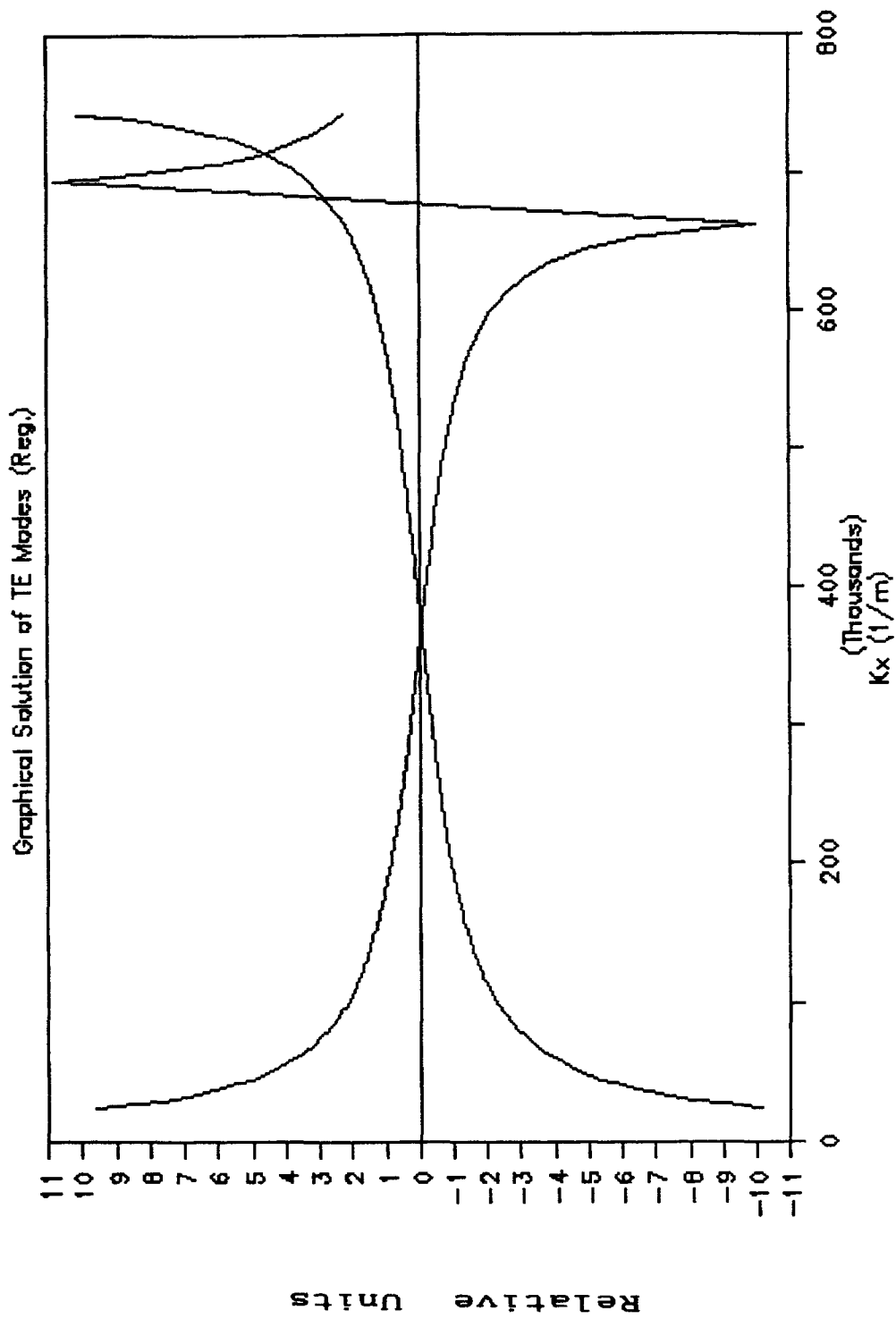
Figure 5.1   Determination of eigenvalues of TE modes
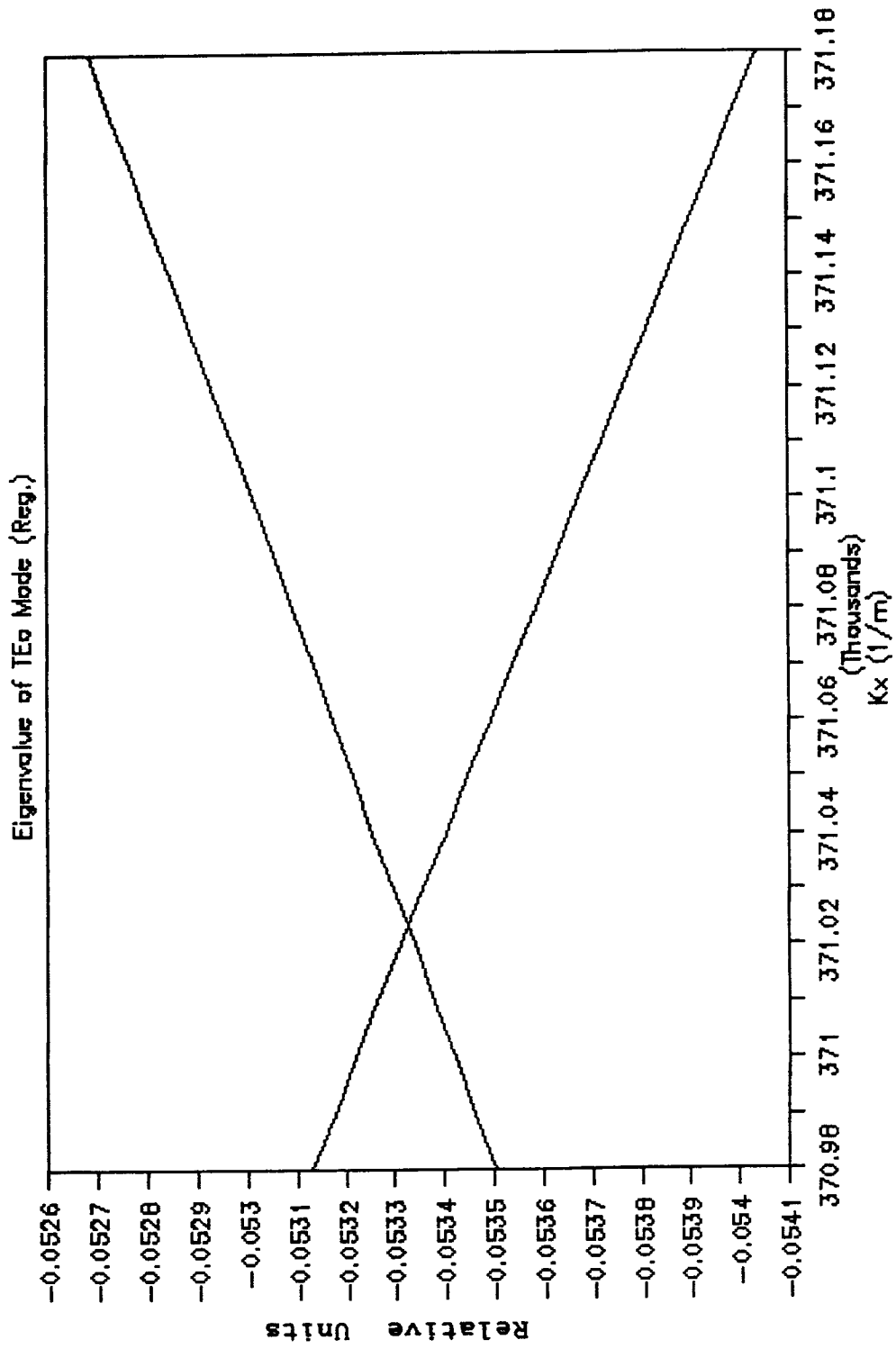by using graphical method, pure PMMA.

Eigenvalue of TEo Mode (Reg.)

Relative Units

Kx (1/m)
(Thousands)

Figure 5.1-(1)   Determine the eigenvalue of TEo mode using
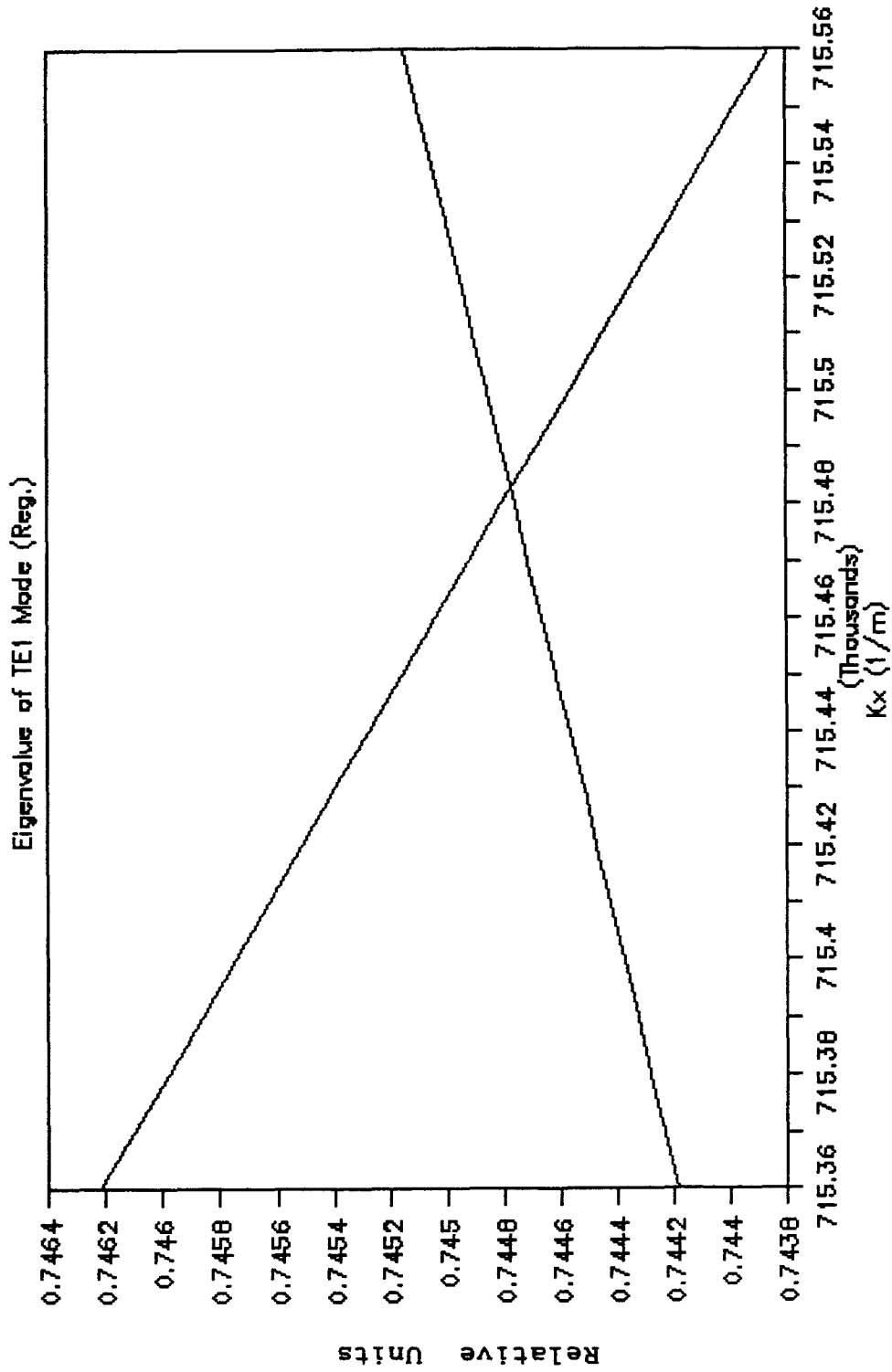the curve magnified from Figure 5.1.

Figure 5.1-(2)   Determine the eigenvalue of TE1 mode using the curve magnified from Figure 5.1.
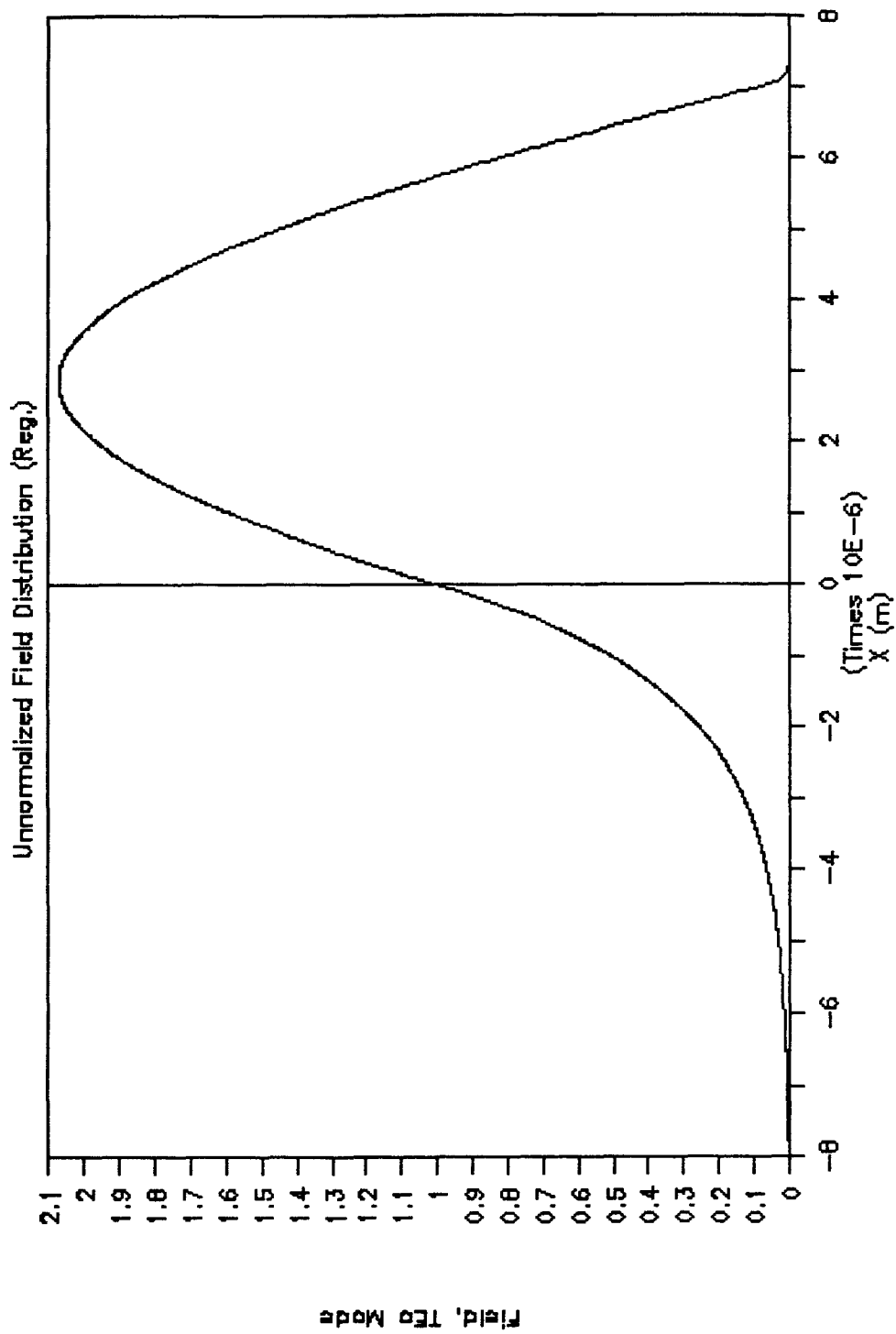
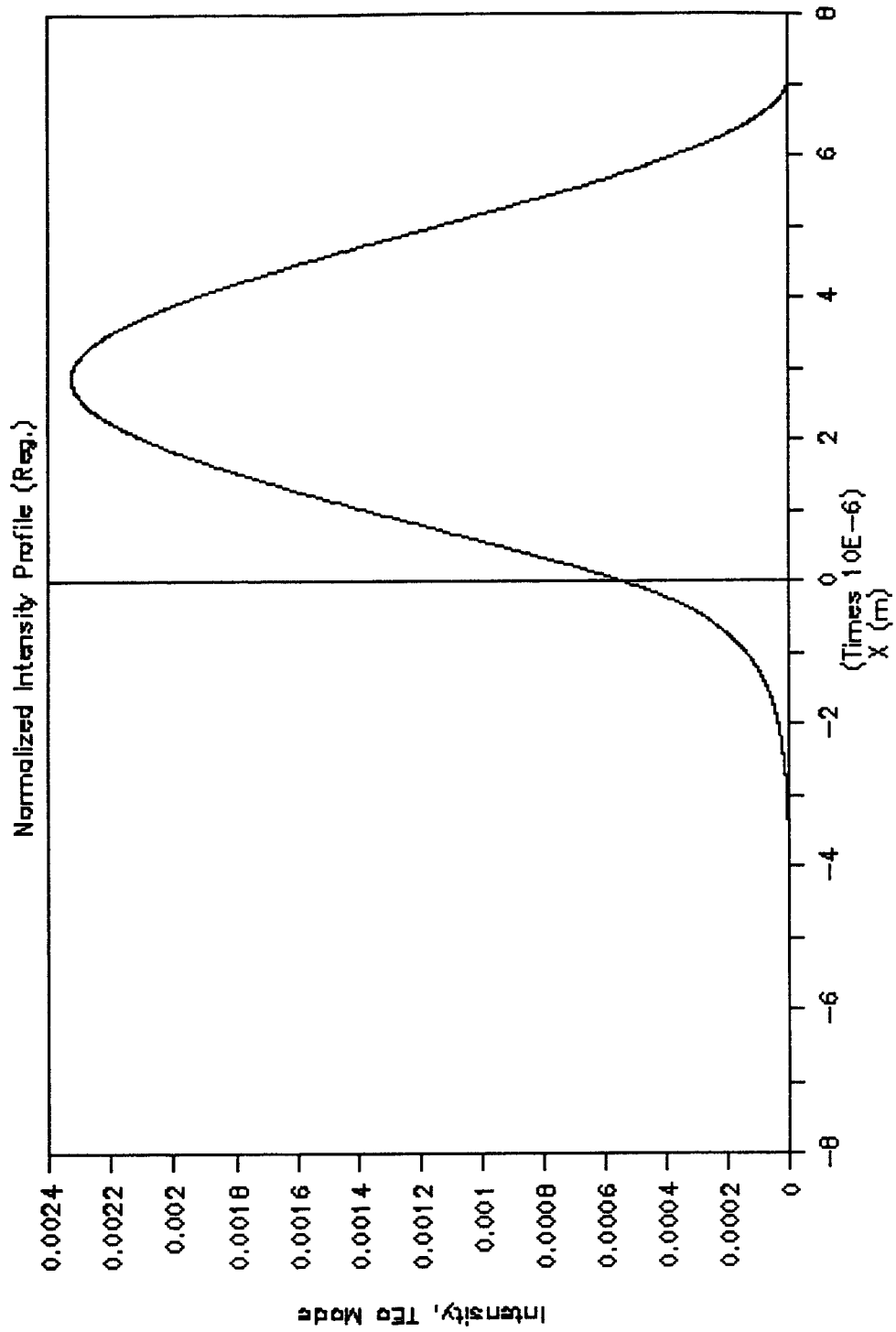Figure 5.2-(1)   Unnormalized Electric field profile of TEo
mode of pure PMMA sample.

Figure 5.2-(2)   Normalized Intensity profile of TEo mode
of pure PMMA sample.
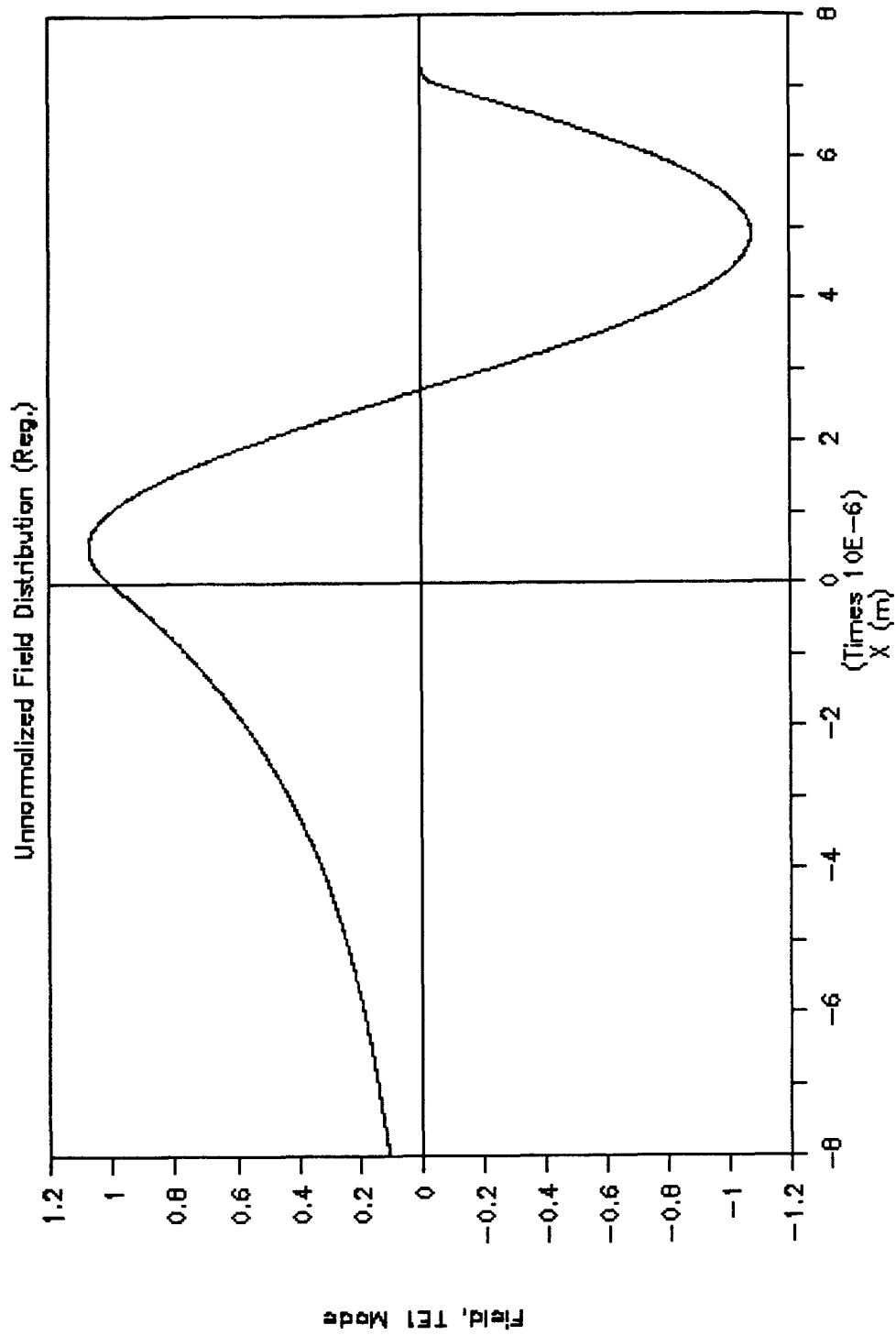
Figure 5.3-(1)   Unnormalized Electric field profile of TE₁
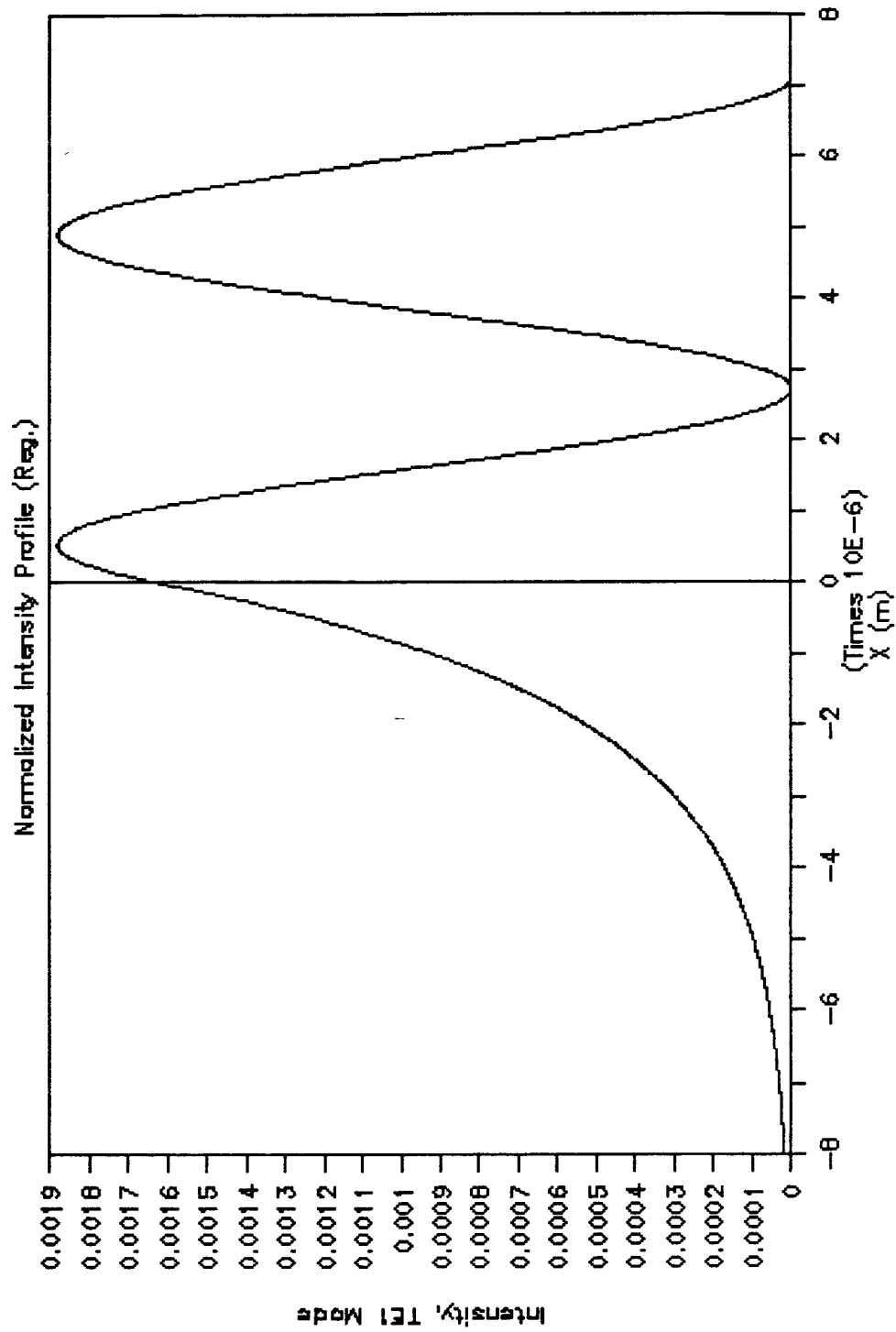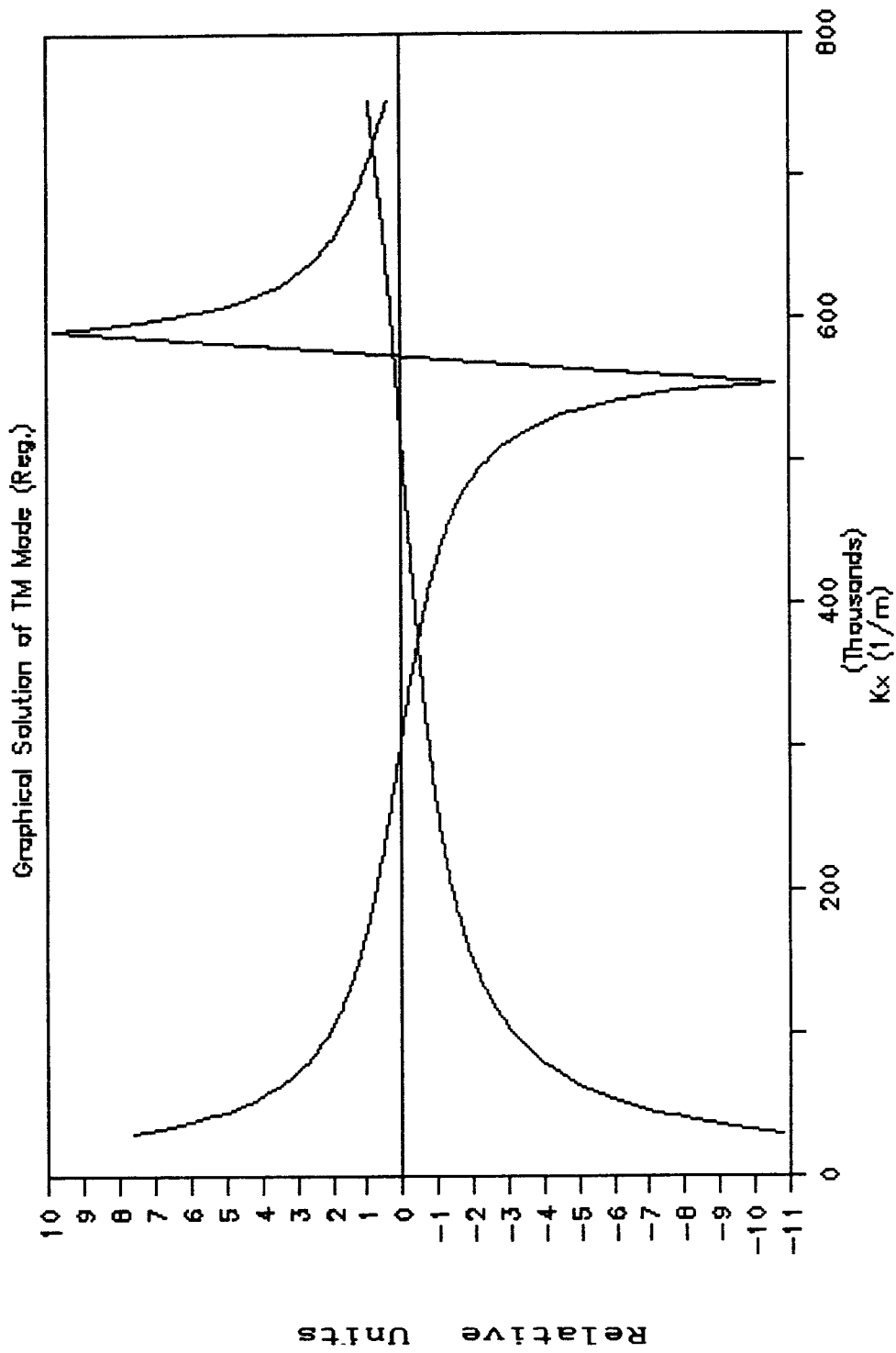mode of pure PMMA sample.

Figure 5.3-(2)   Normalized Intensity profile of TE1 mode
of pure PMMA sample.

Figure 5.4   Determination of eigenvalues of TM modes
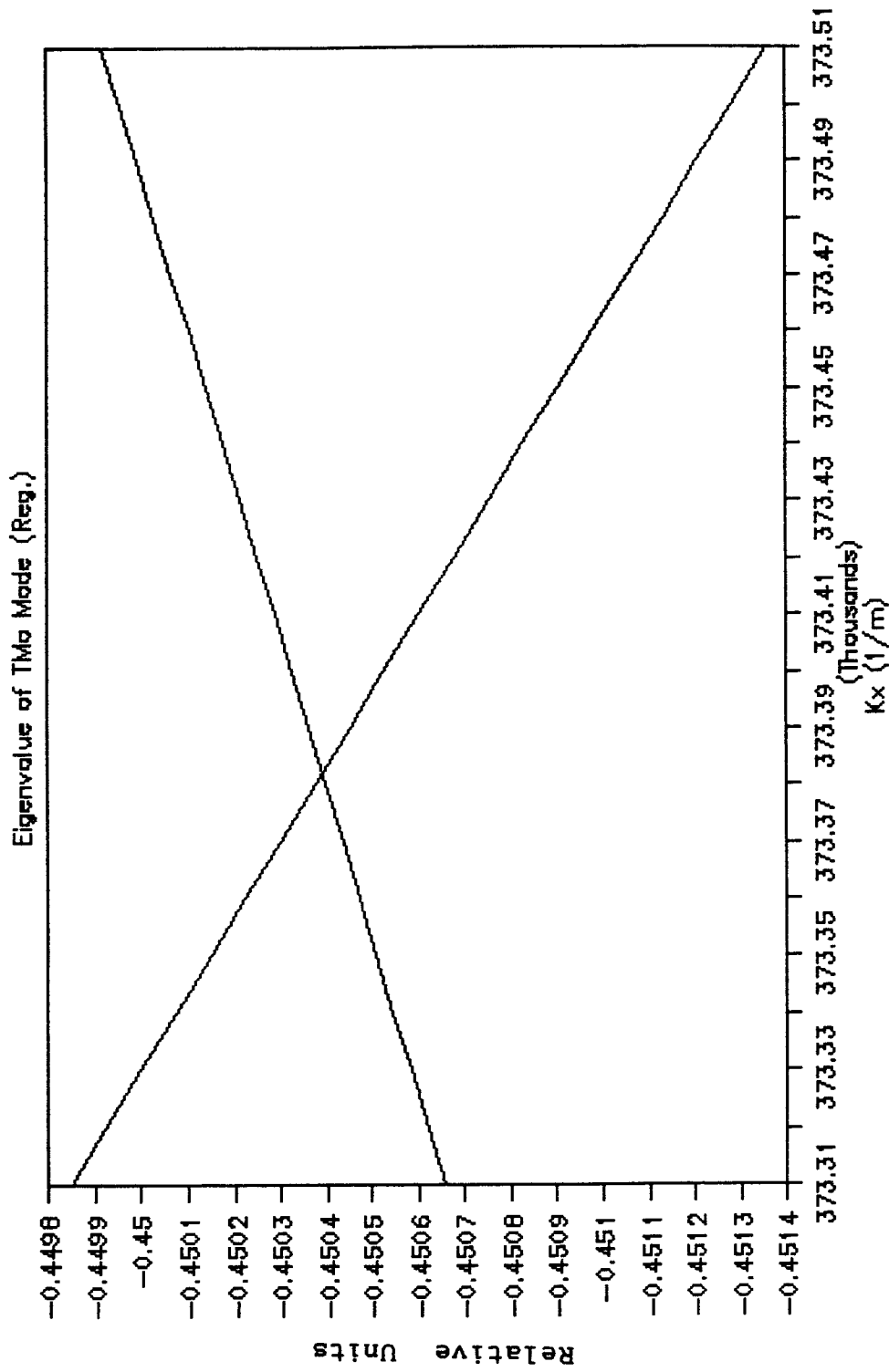by using graphical method, pure PMMA.

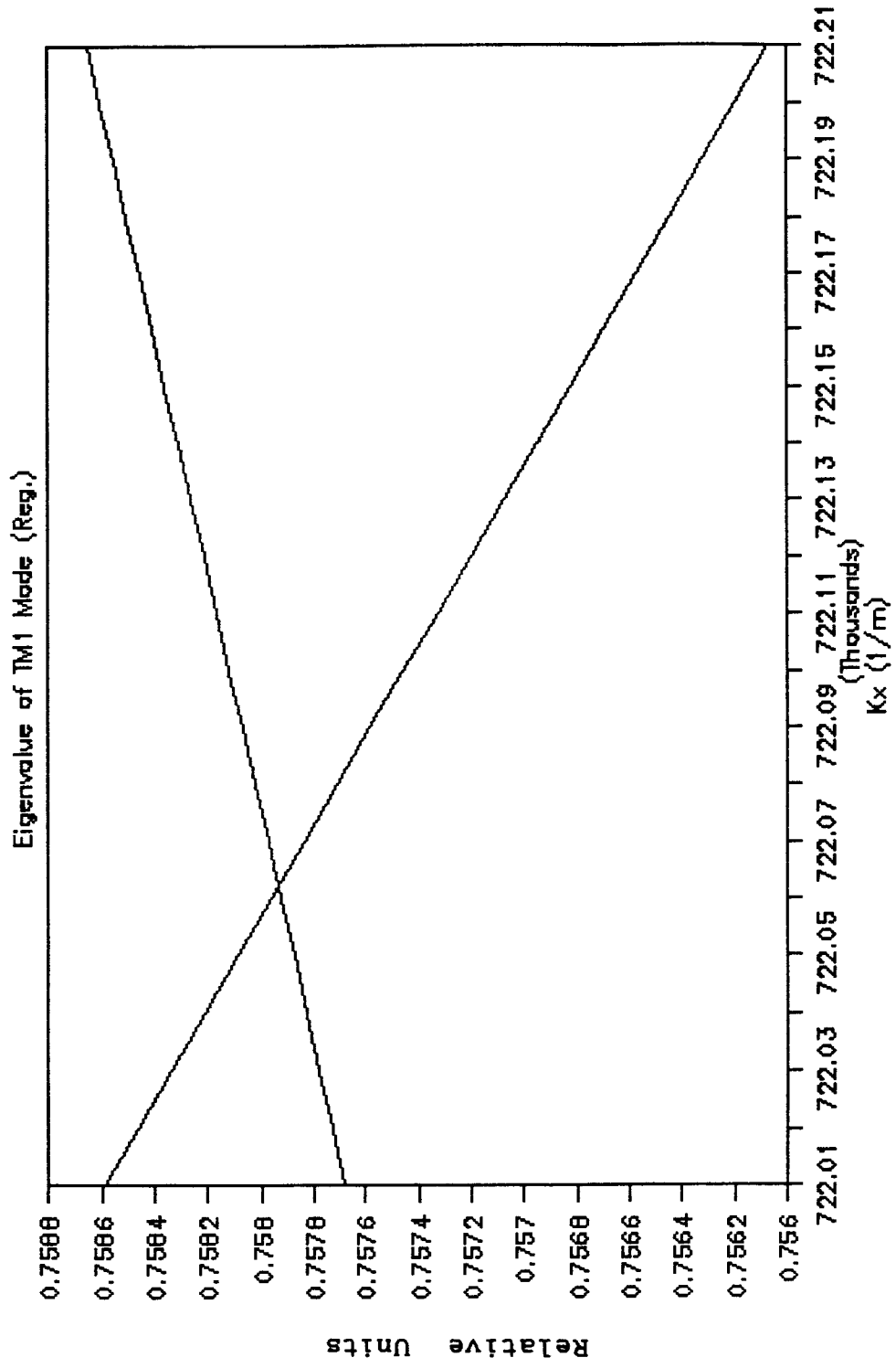*Figure 5.4-(1)* Determine the eigenvalue of TMo mode using the curve magnified from Figure 5.4.

Figure 5.4-(2) Determine the eigenvalue of TM1 mode using the curve magnified from Figure 5.4.
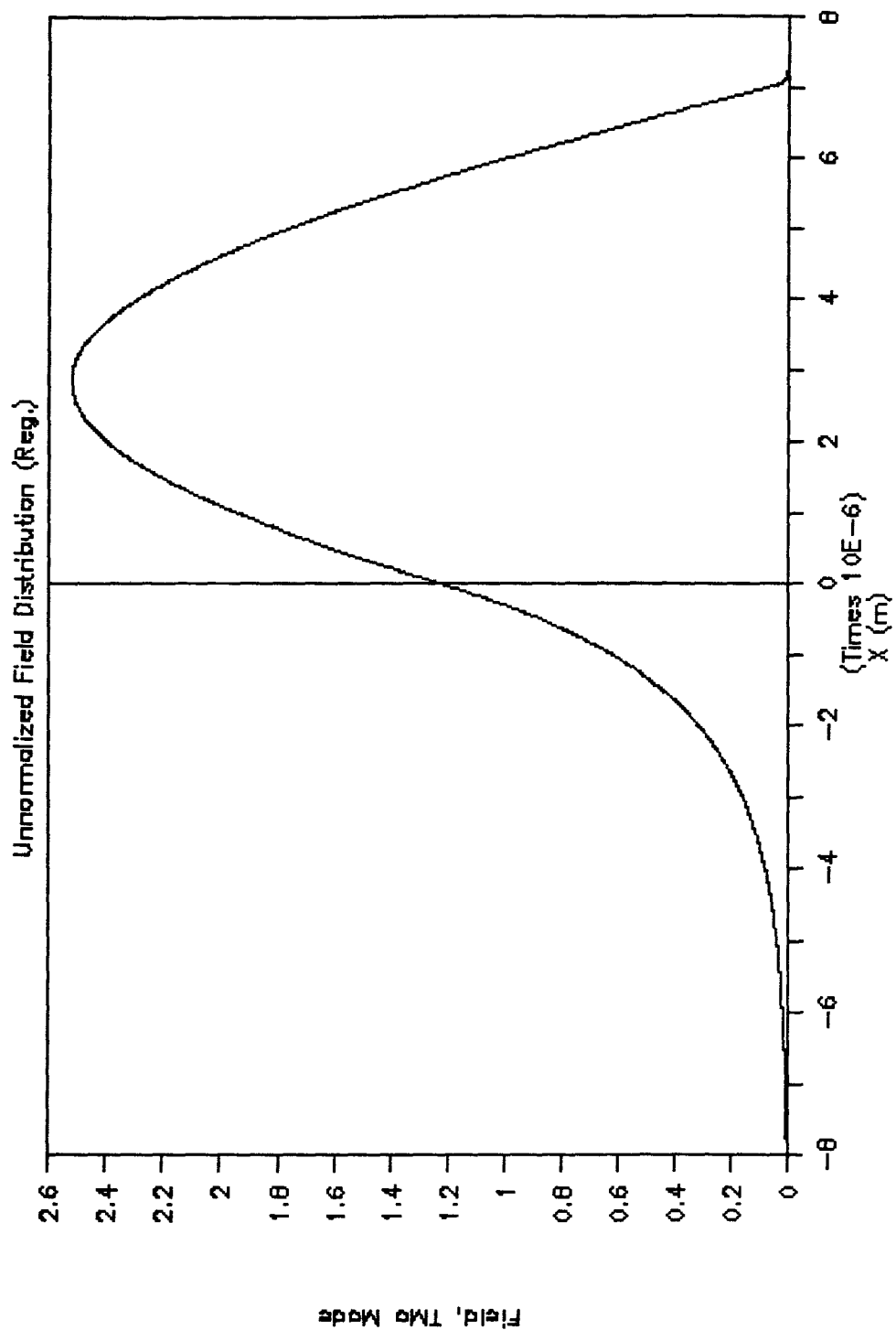
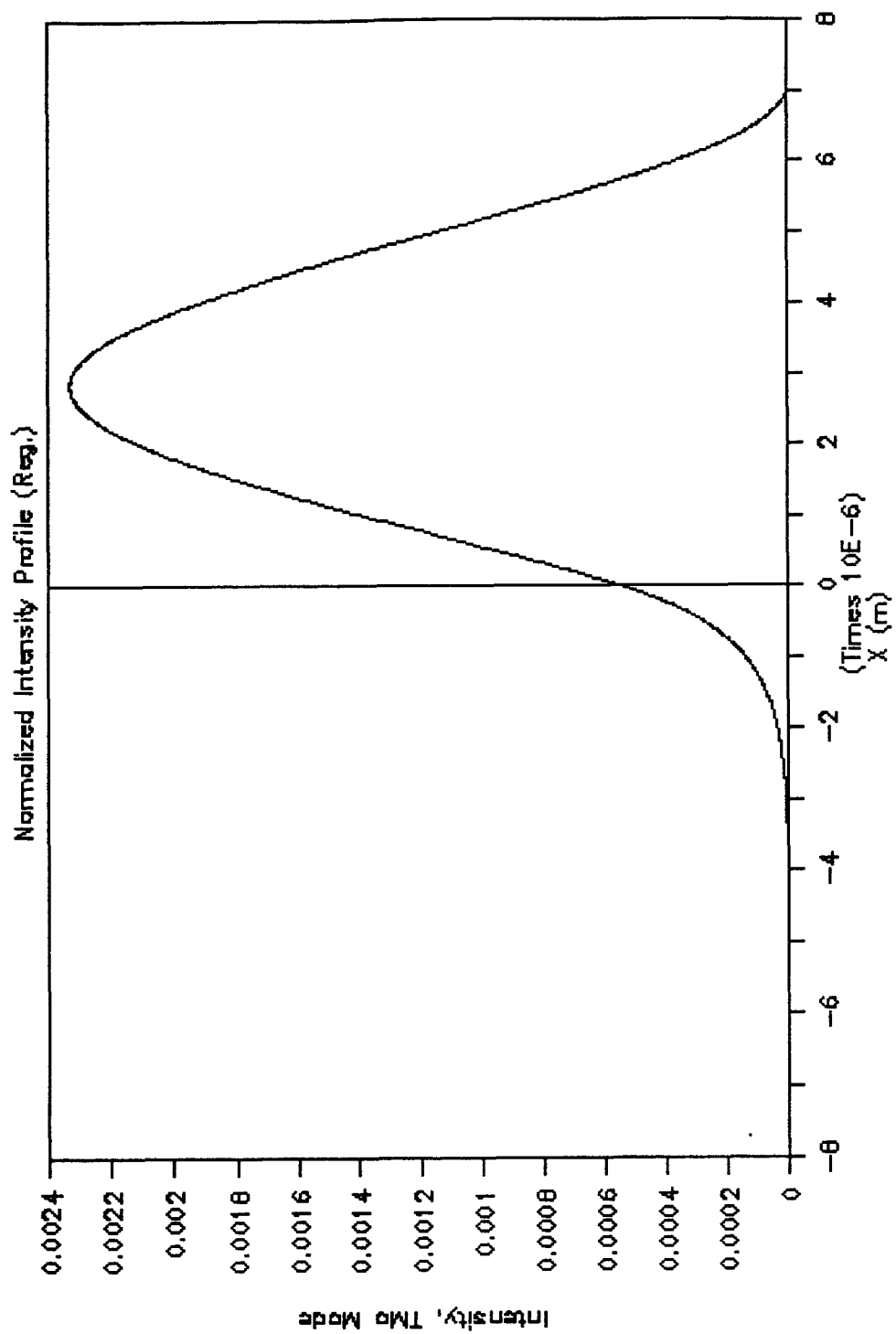*Figure 5.5-(1)*   Unnormalized Electric field profile of TMo mode of pure PMMA sample.

Figure 5.5-(2)   Normalized Intensity profile of TMo mode
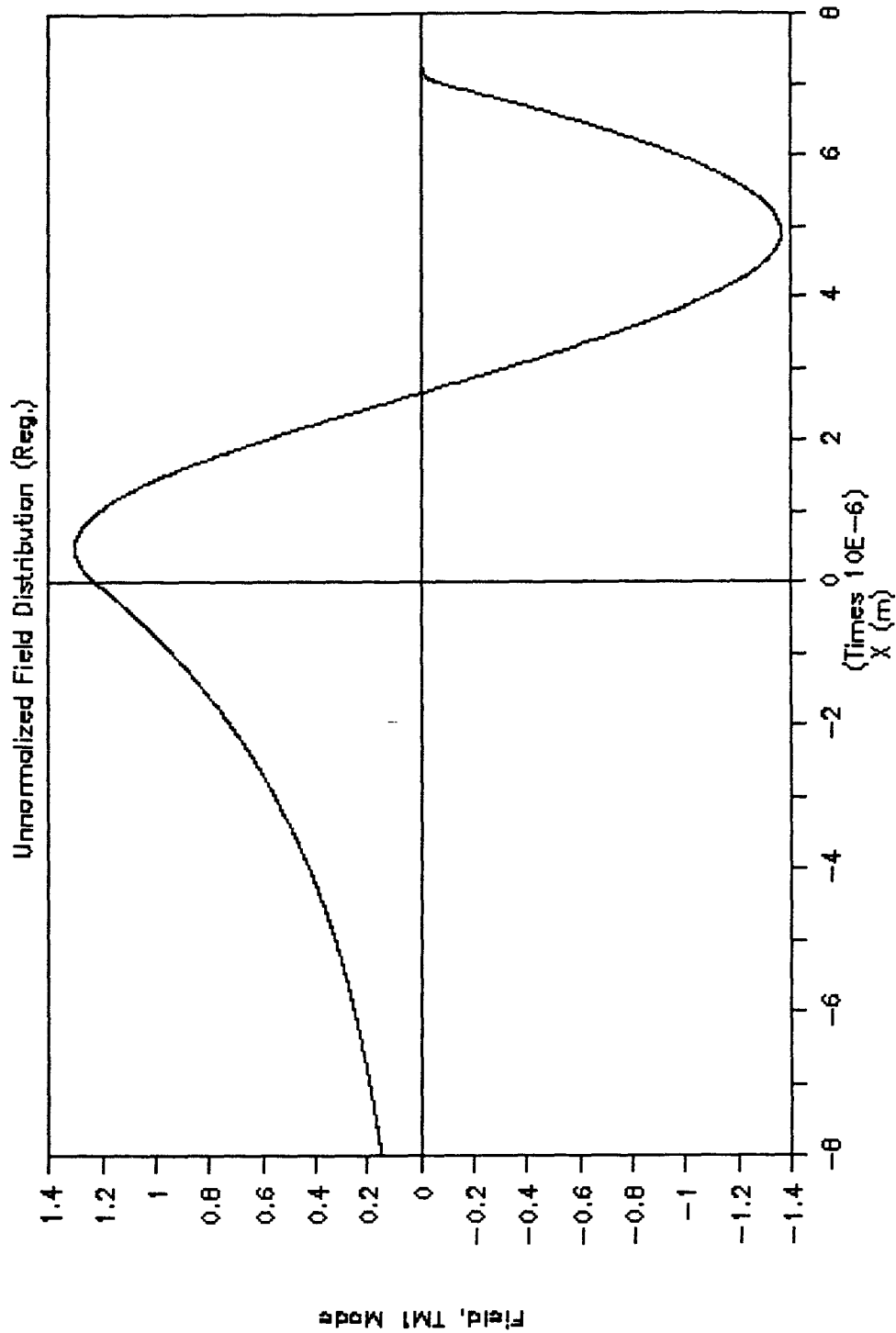of pure PMMA sample.

Figure 5.6-(1)   Unnormalized Electric field profile of TM₁ mode of pure PMMA.

Figure 5.6-(2)   Normalized Intensity profile of TM1 mode
of pure PMMA sample.

Graphical Solution of TE Modes (Al)

K_x (Thousands) (1/m)

Relative Units

Figure 5.7   Determination of eigenvalues of TE modes by suing graphical method, APMPG structure sample.

52

Figure 5.7-(1) Determine the eigenvalue of TEo mode using the curve magnified from Figure 5.7.

Figure 5.7-(2)   Determine the eigenvalue of TE1 mode using the curve magnified from Figure 5.7.

Figure 5.8-(1)   Unnormalized Electric field profile of TEo mode of APMPG structure sample.

Figure 5.8-(2)   Normalized Intensity profile of TEo mode
of APMPG structure sample.

Figure 5.9-(1)   Unnormalized Electric field profile of TE₁ mode of APMPG structure sample.
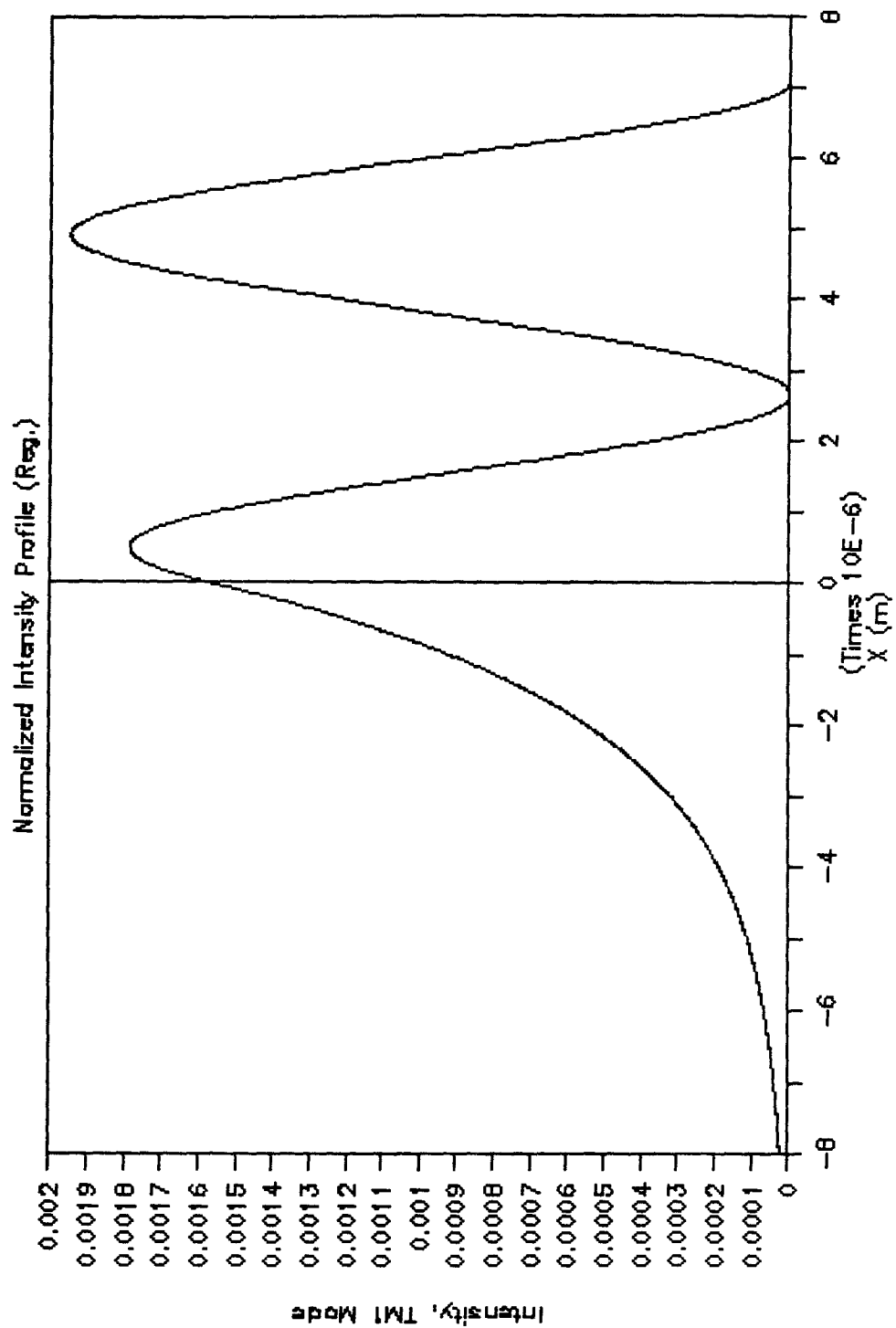
Figure 5.9-(2)   Normalized Intensity profile of TE1 mode
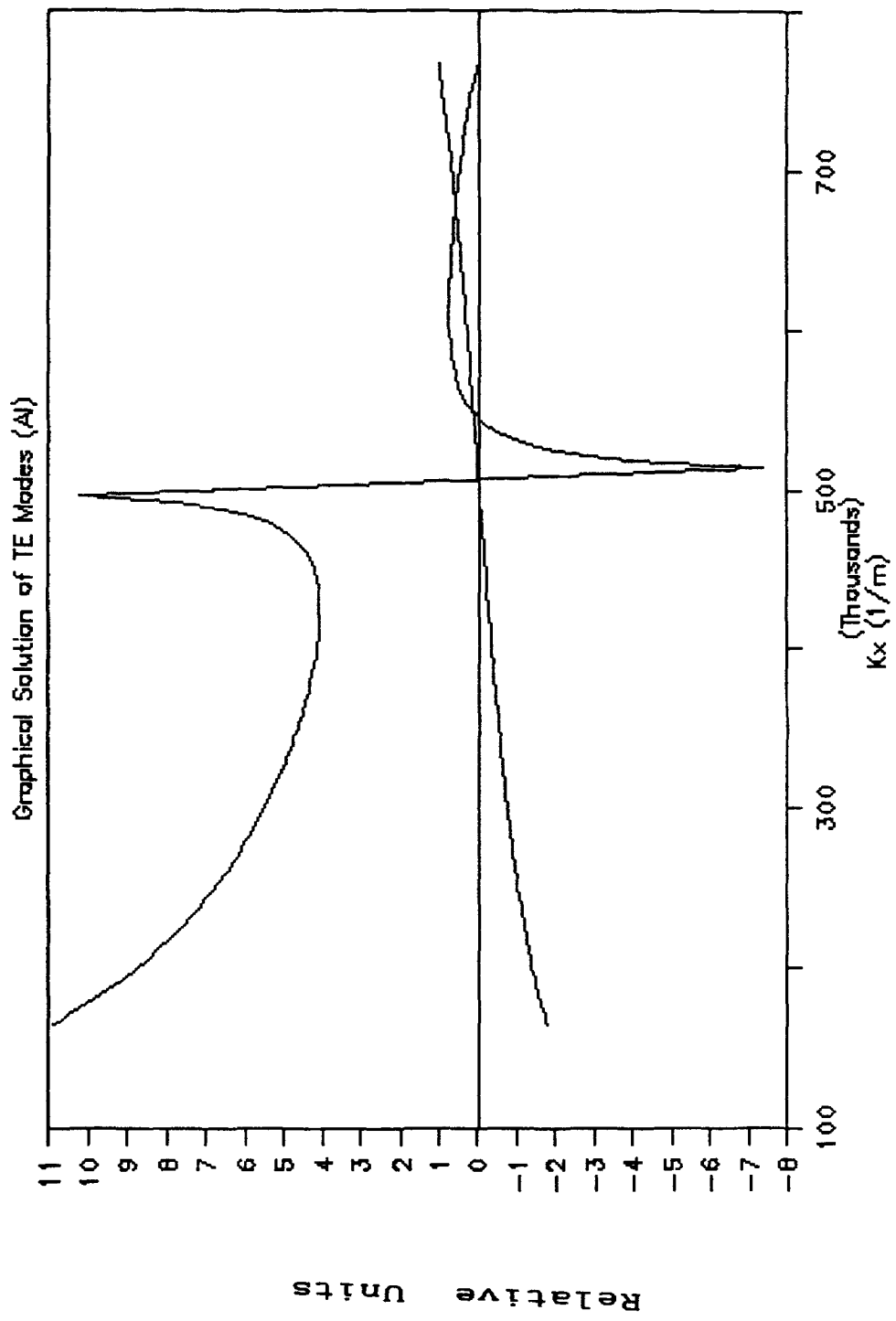of APMPG structure sample.
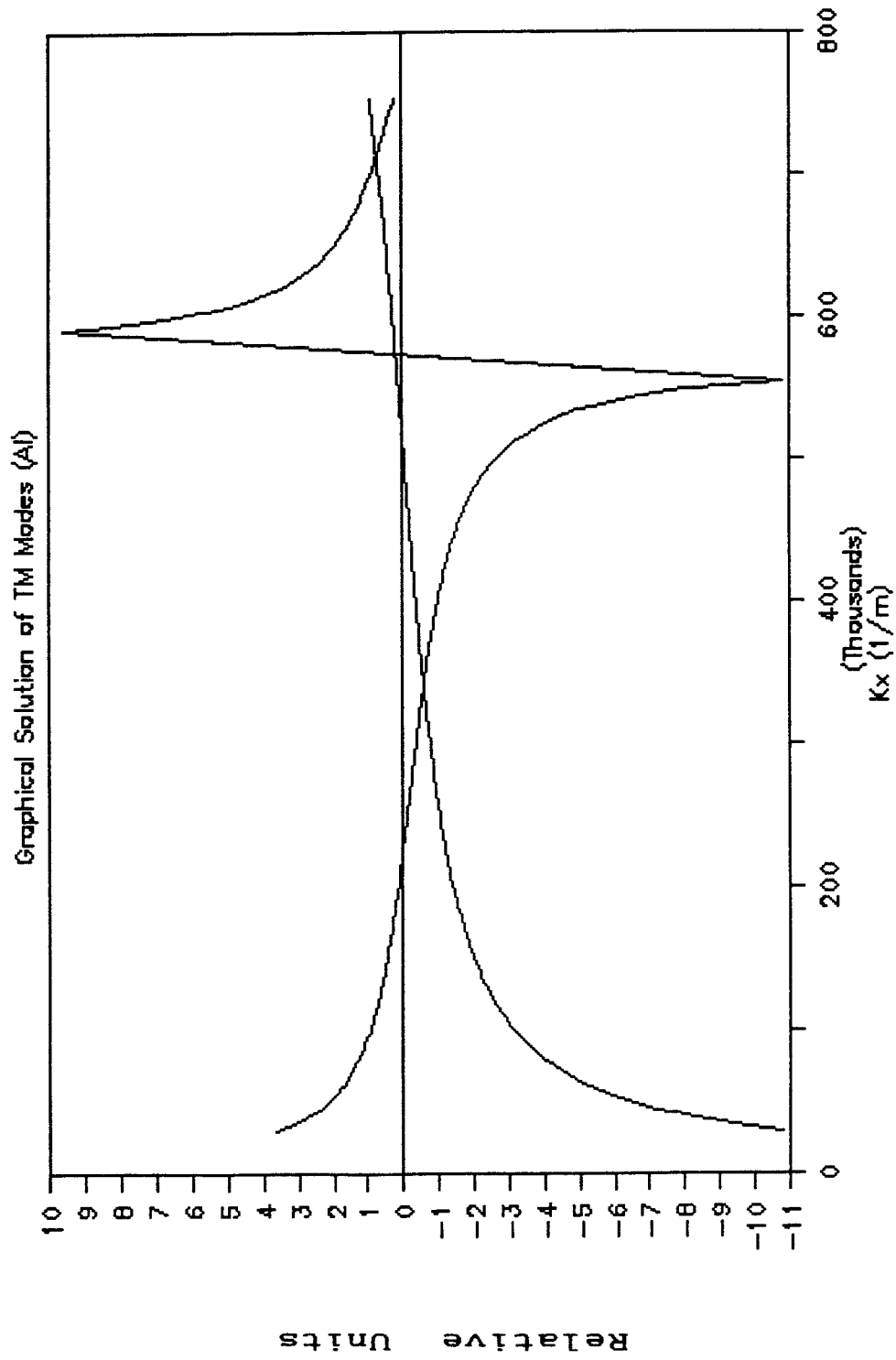
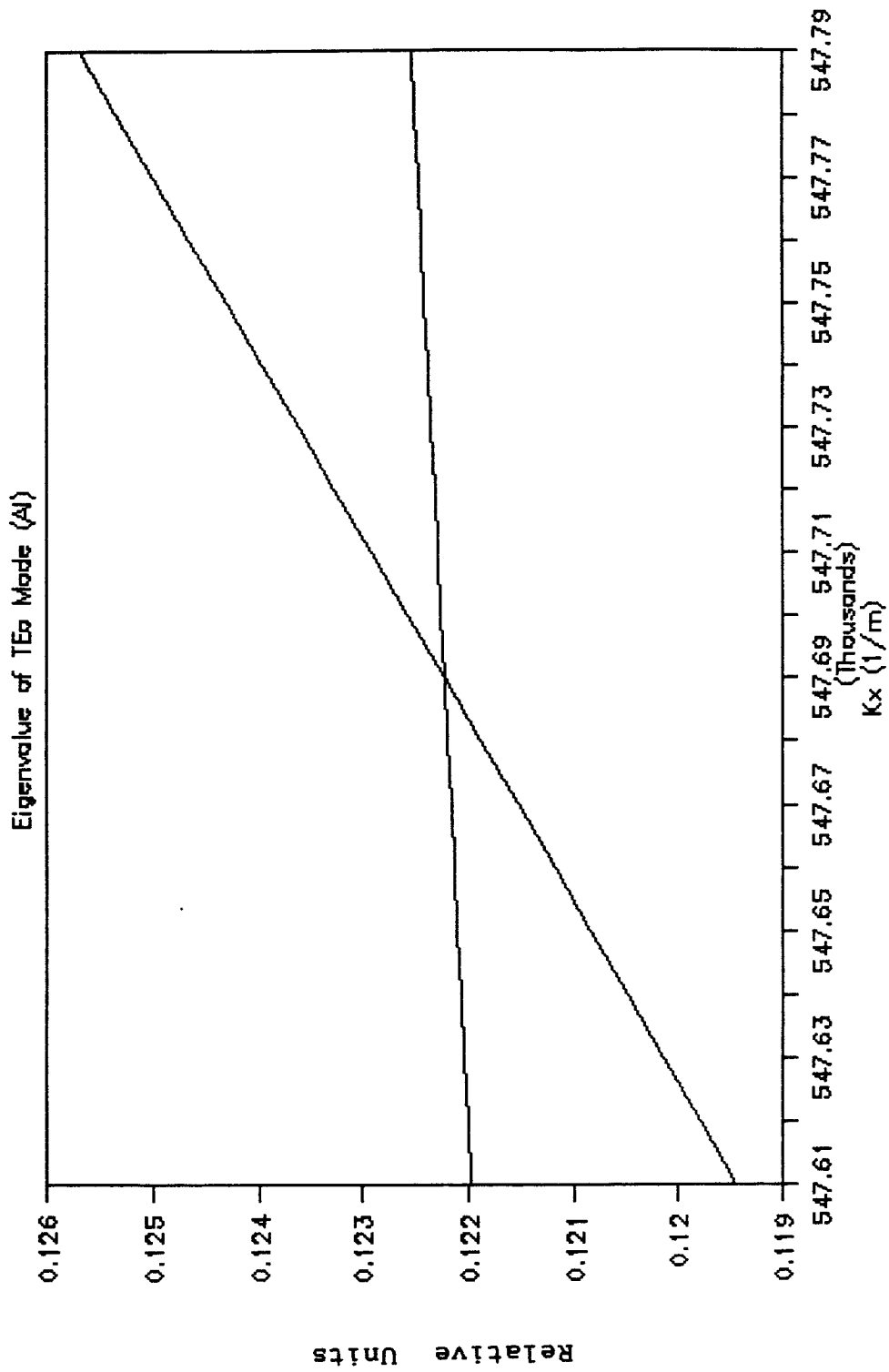*Figure 5.10* Determination of eigenvalues of TM modes by using graphical method, APMPG structure sample.
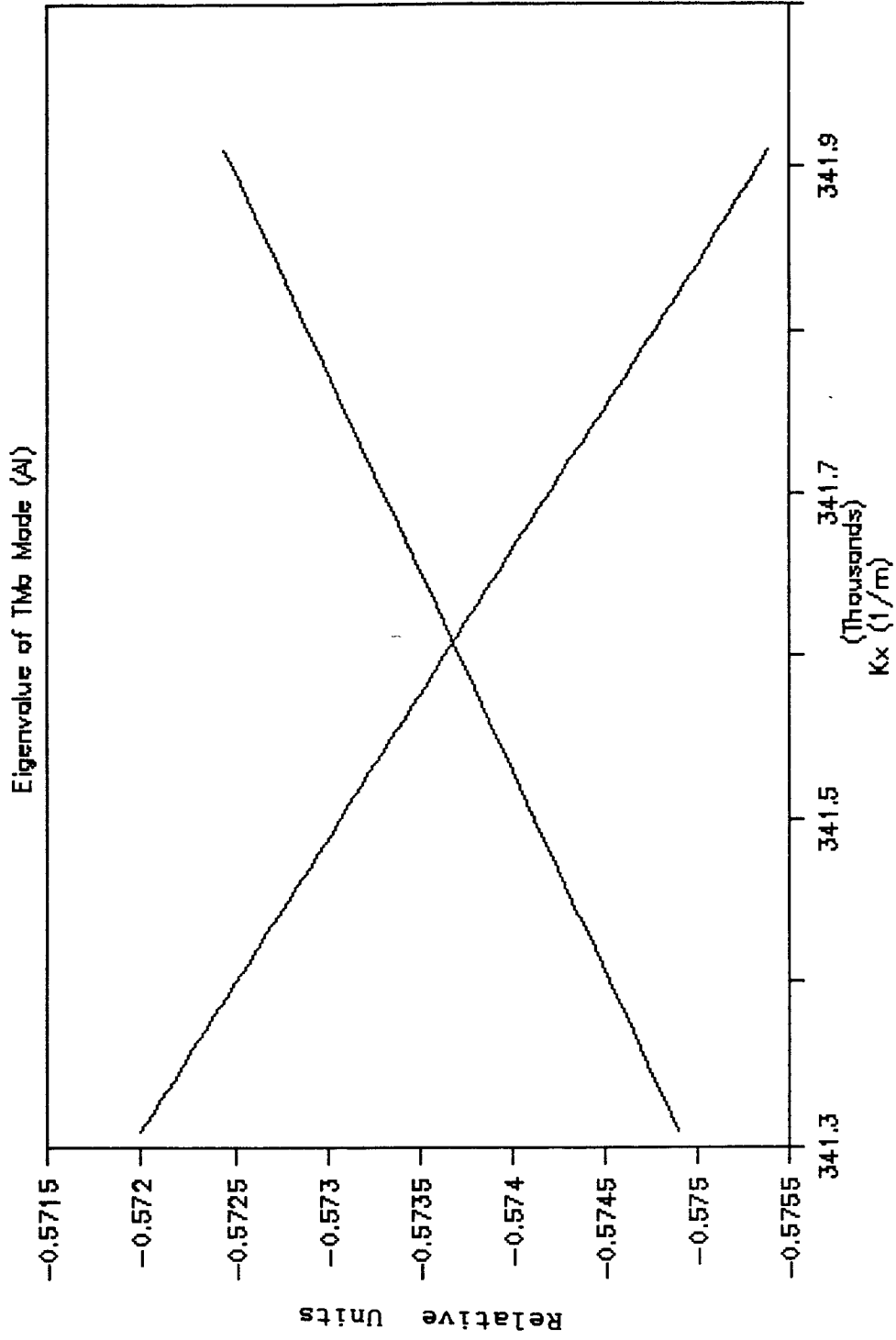
Figure 5.10-(1)   Determine the eigenvalue of TMo mode using the curve magnified from Figure 5.10.
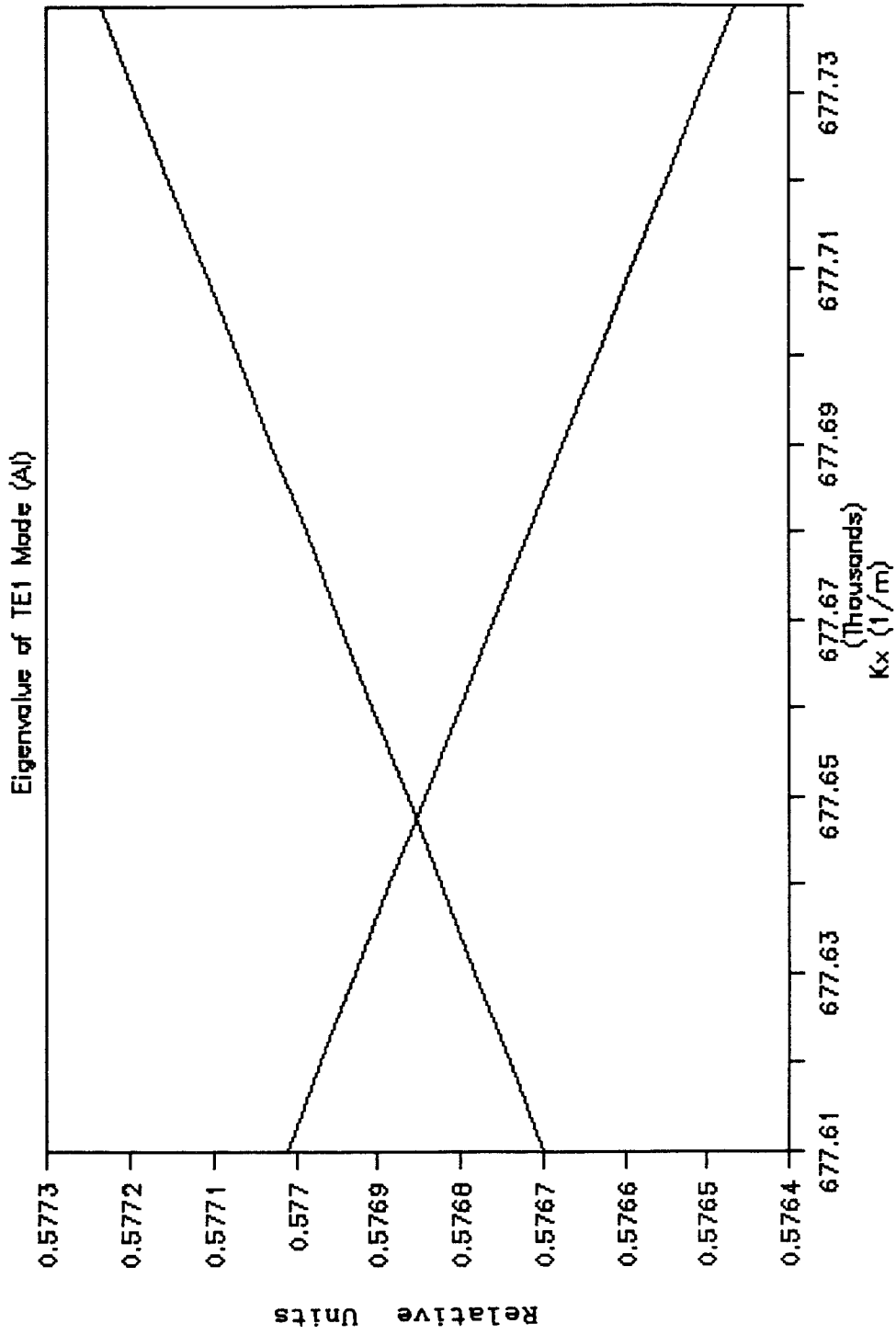
Eigenvalue of TM1 Mode (Al)

Kx (1/m)
(Thousands)

Relative Units
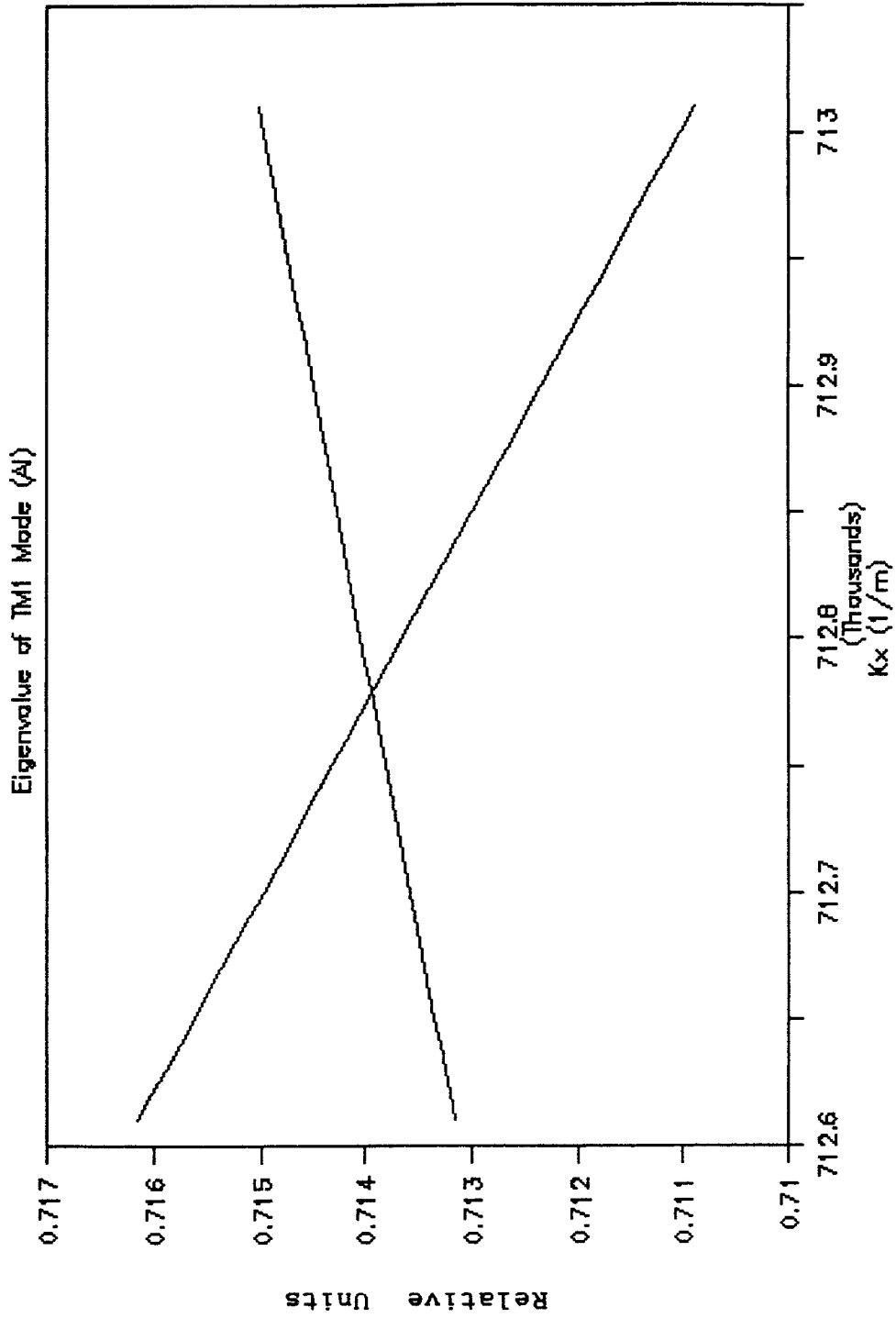
Figure 5.10-(2)   Determine the eigenvalue of TM1 mode using the curve magnified from Figure 5.10.

Figure 5.11-(1) Unnormalized Electric field profile of TMo mode of APMPG structure sample.

Figure 5.11-(2)   Normalized Intensity profile of TMo mode
of APMPG structure sample.
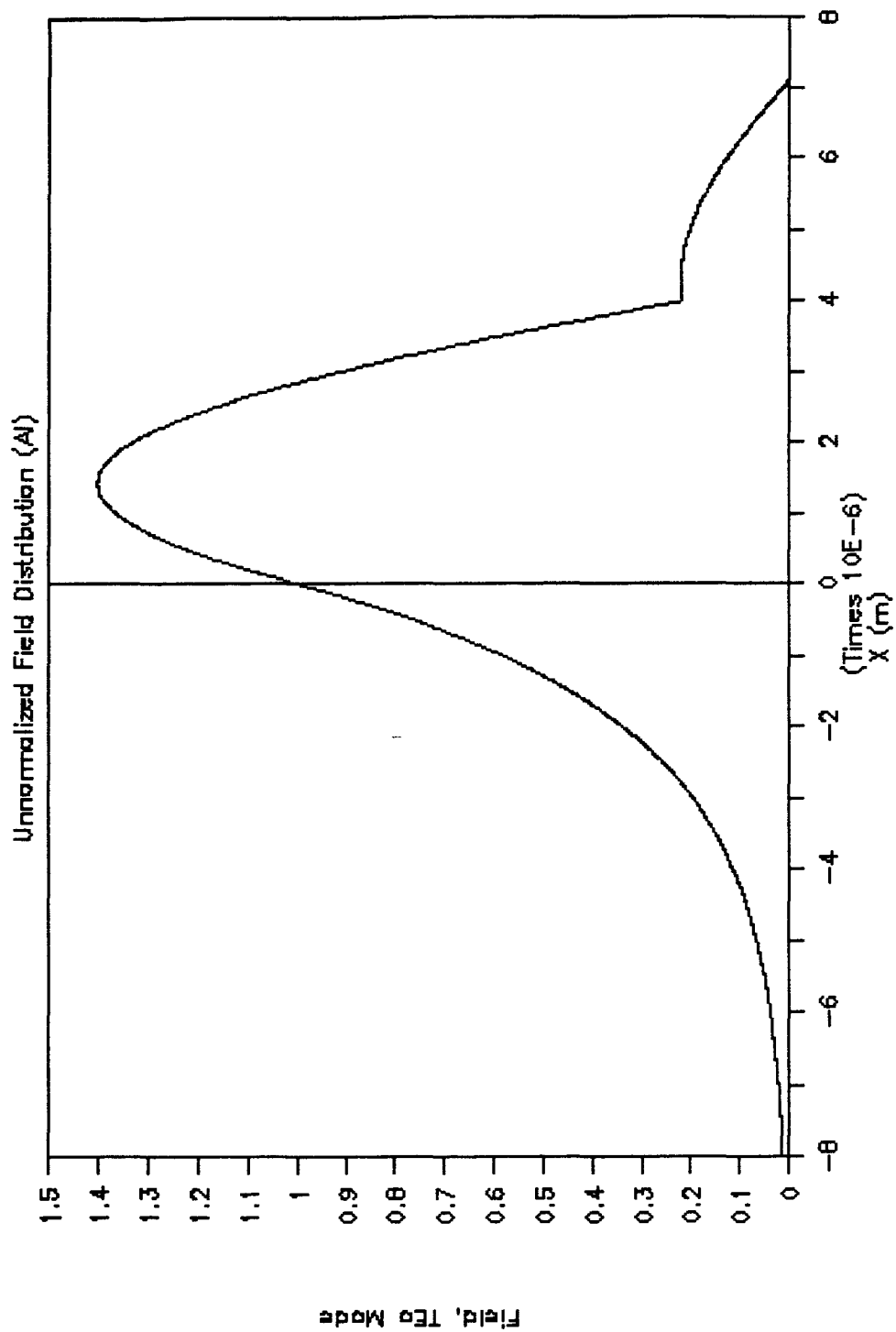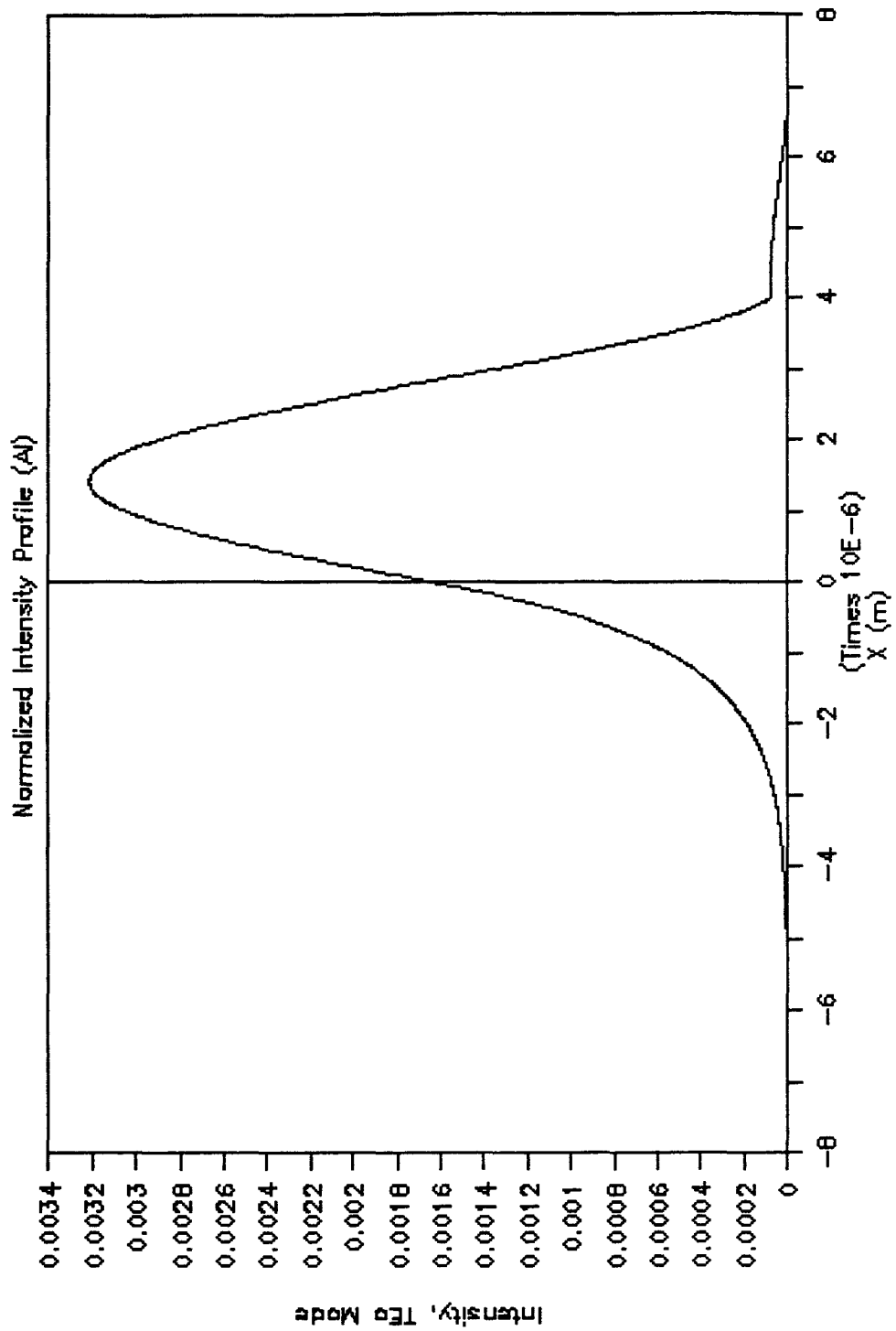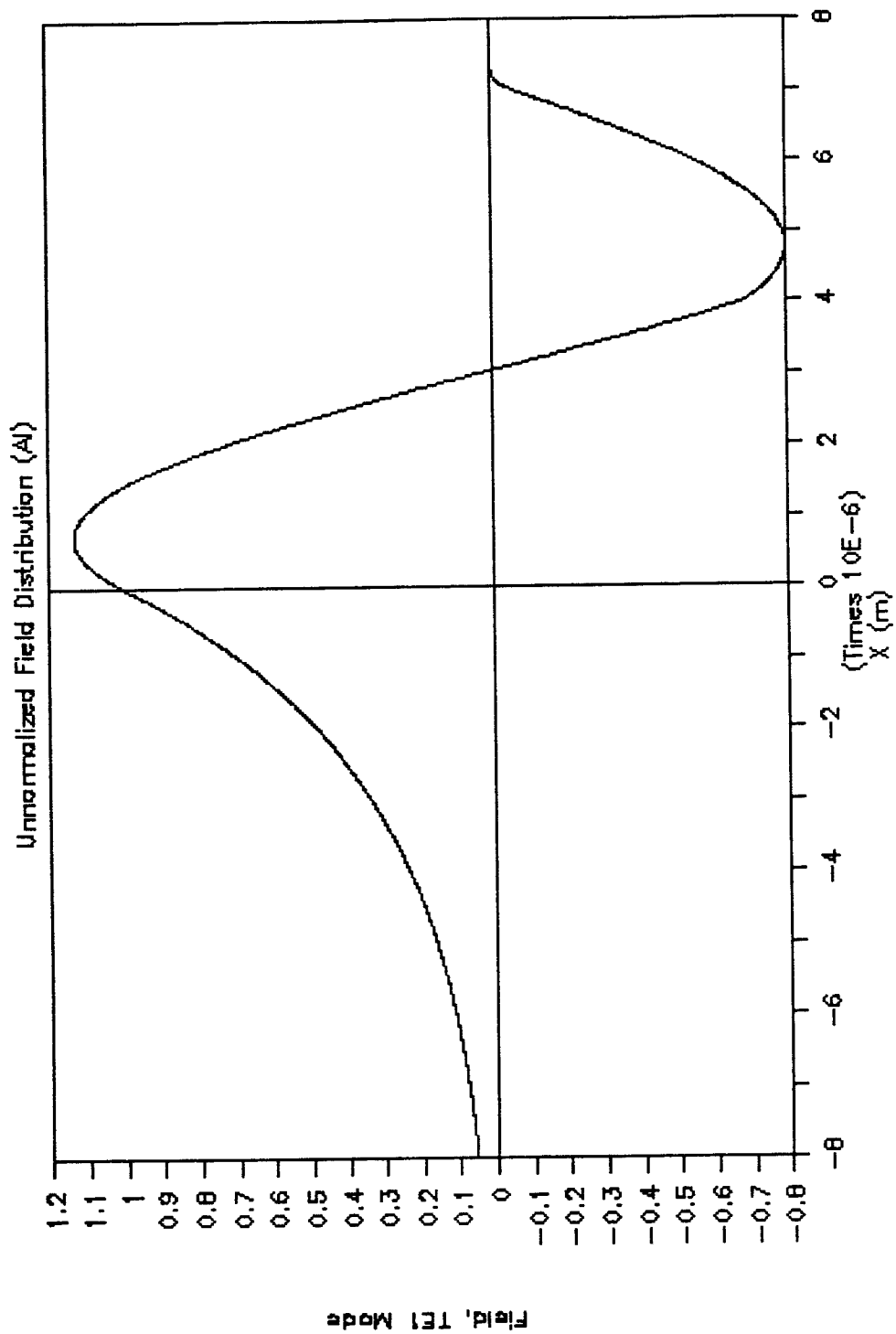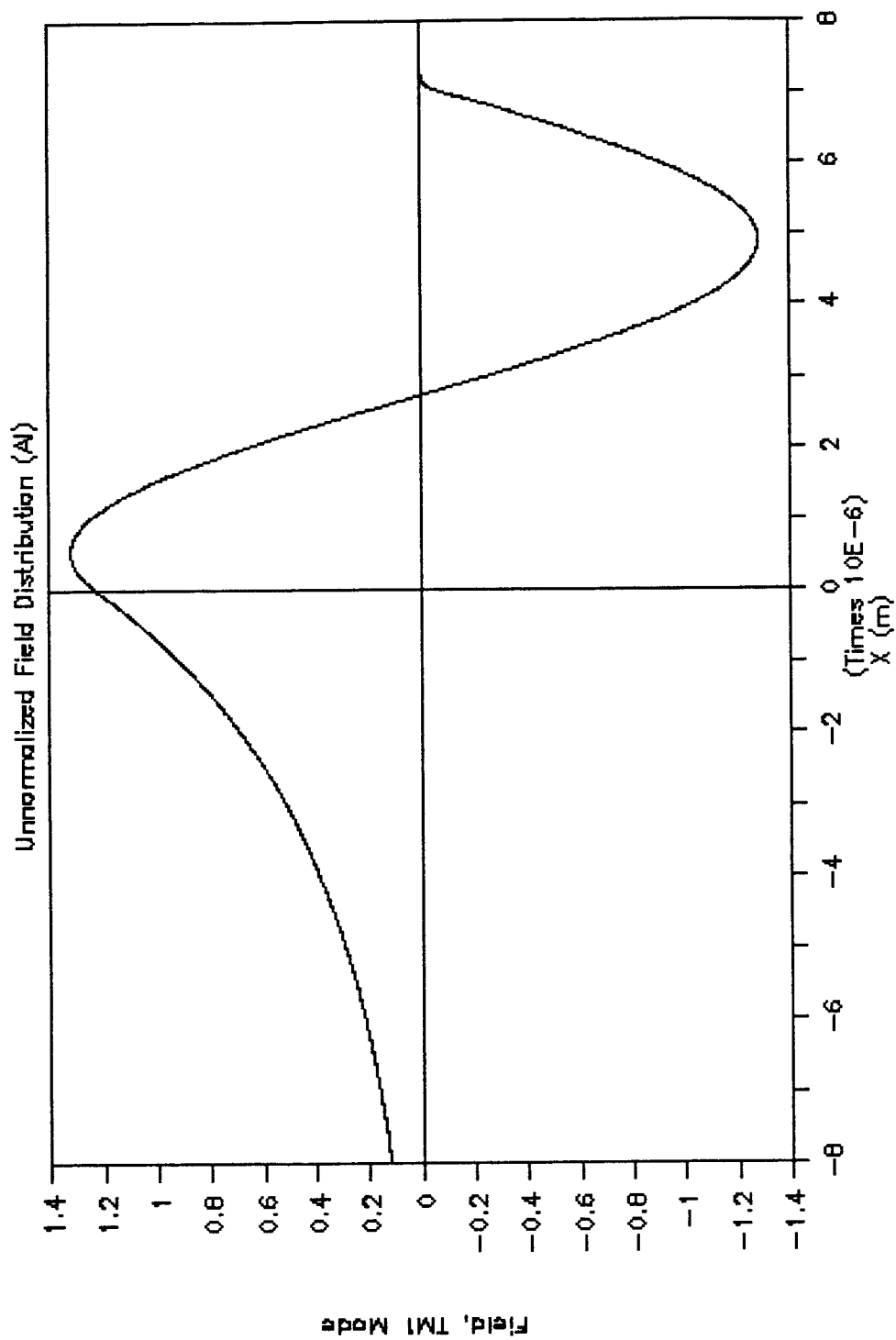
Figure 5.12-(1)   Unnormalized Electric field profile of TM₁
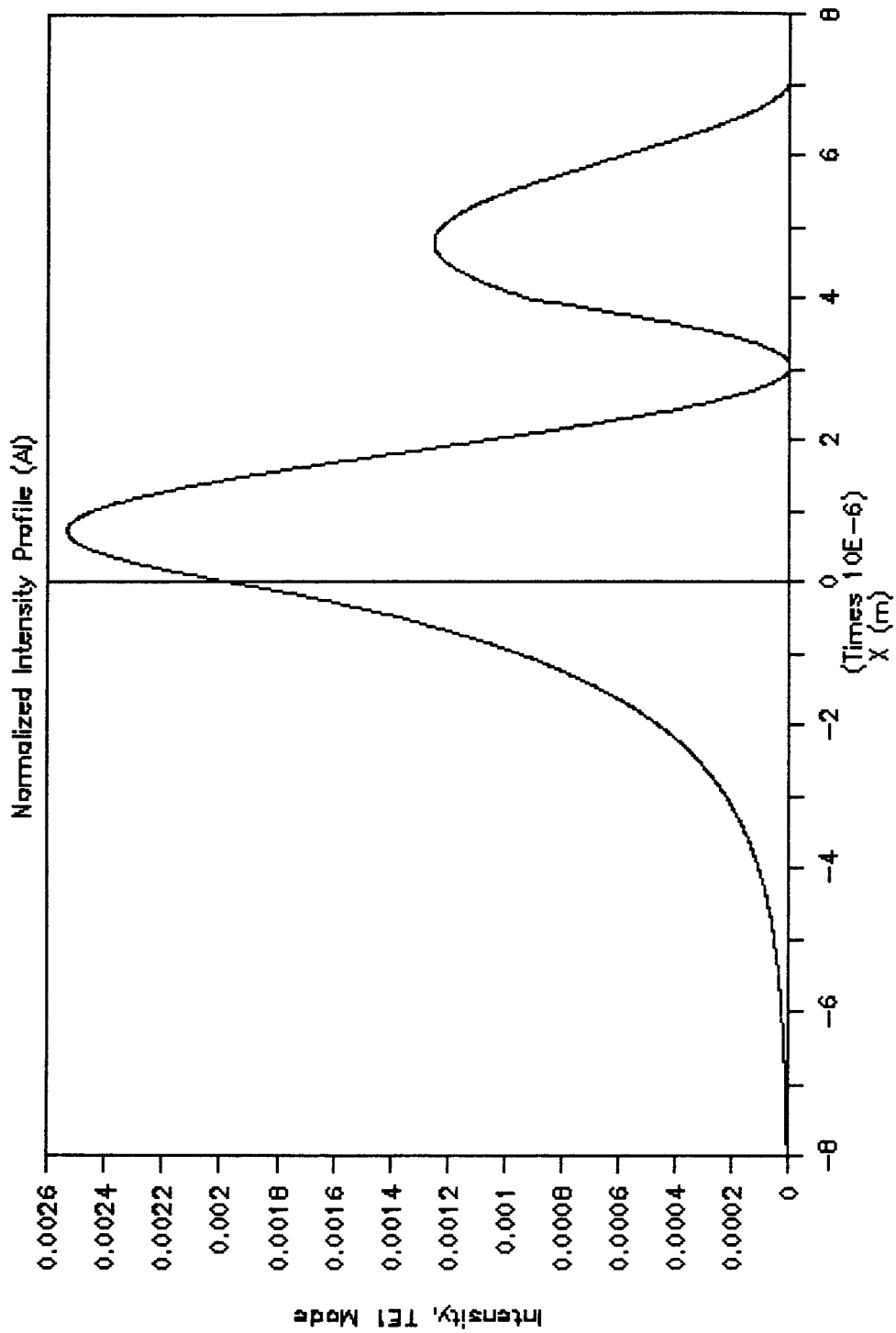mode of AMPMG structure sample.
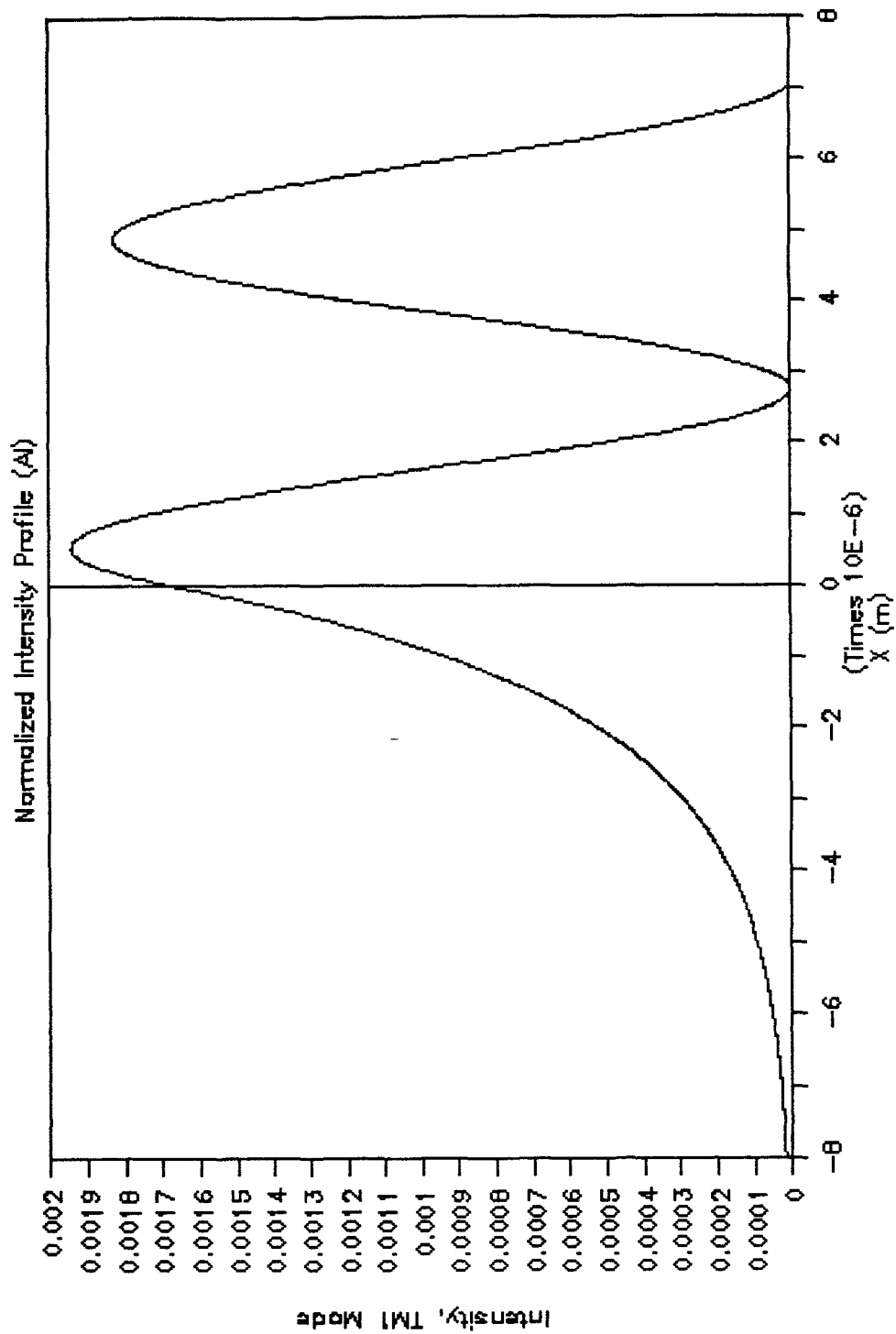
Figure 5.12-(2) Normalized Intensity profile of TM₁ mode of APMPG structure sample.

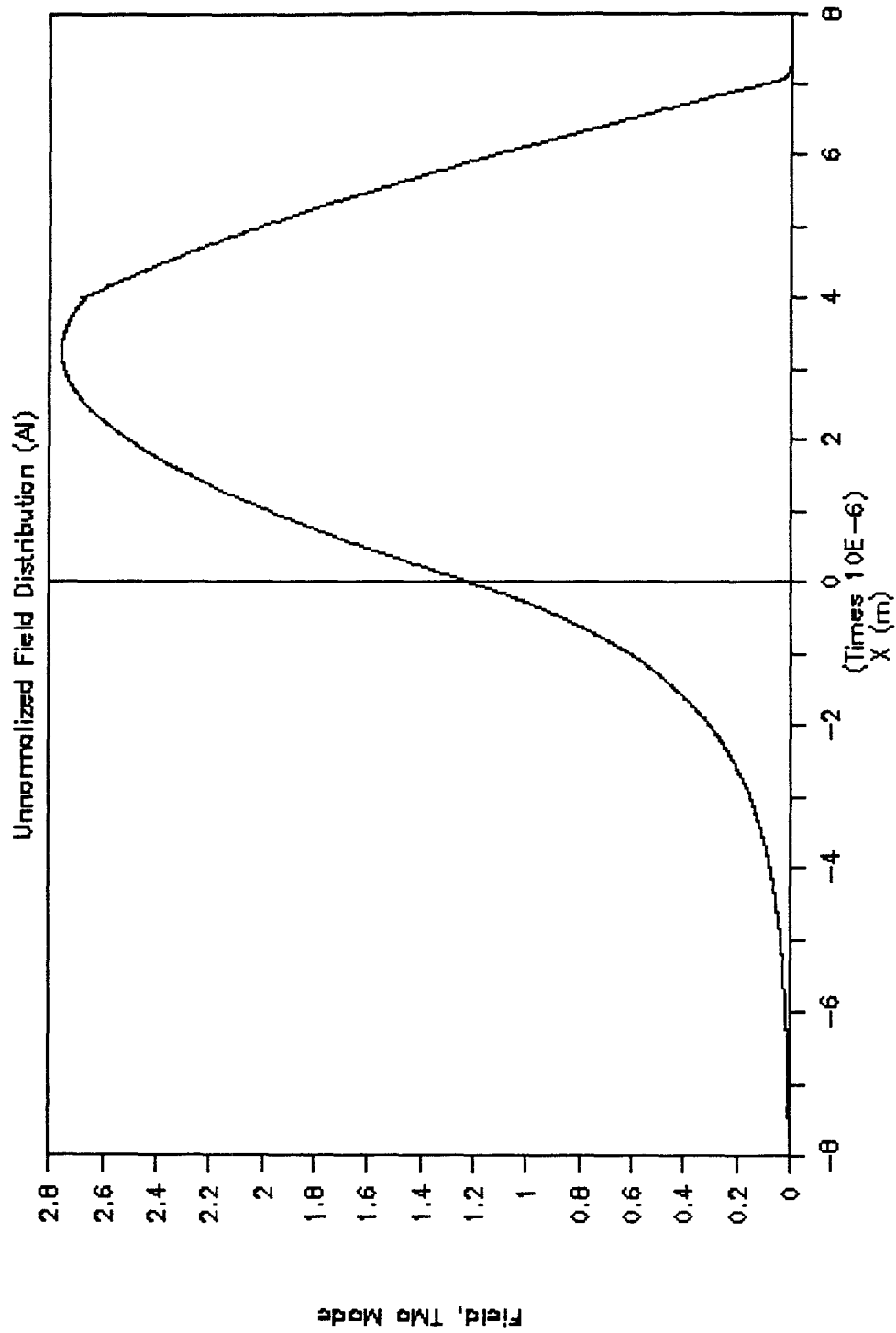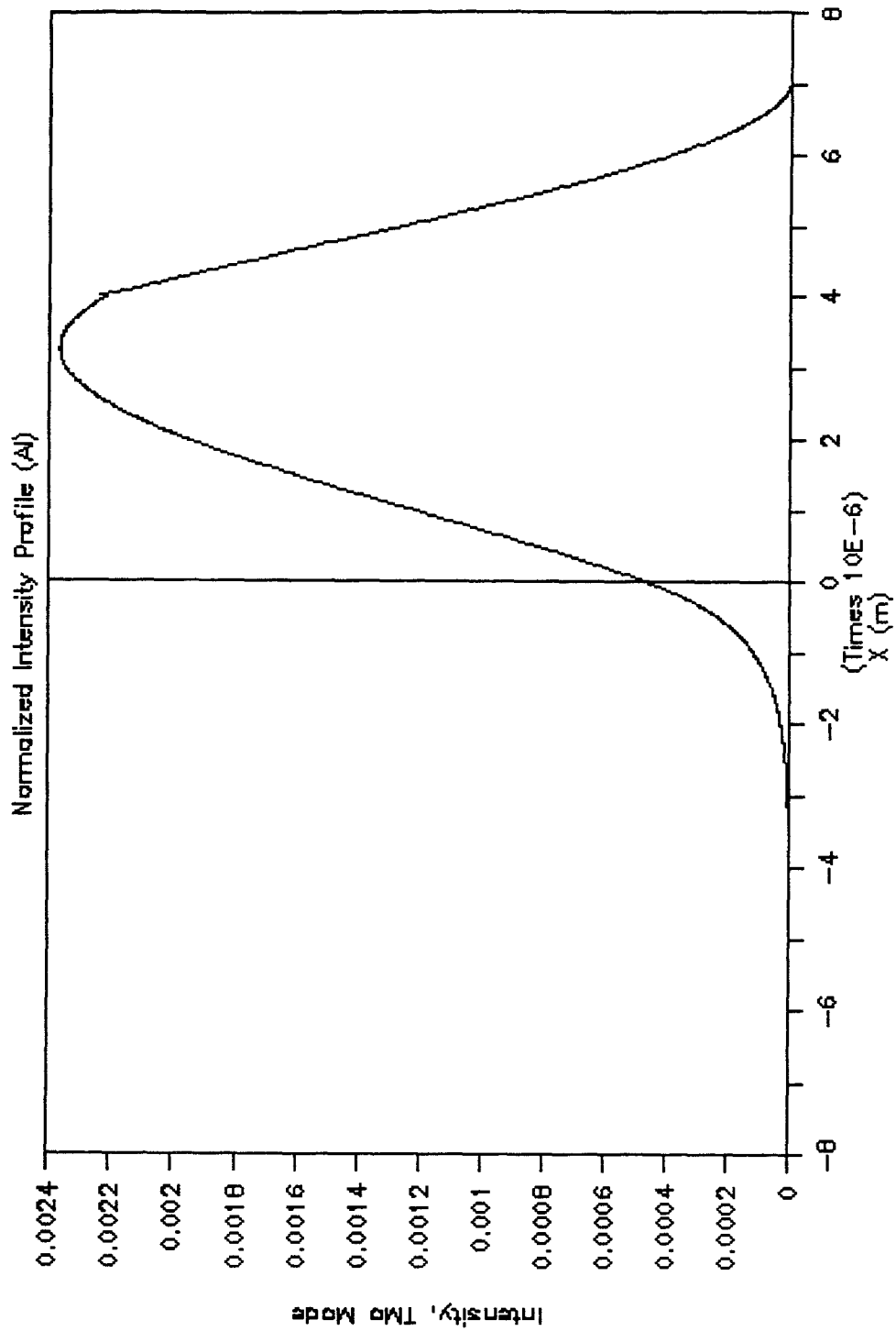smaller ($\Delta N_{g,p}$ = 1.500-1.496 = 0.004) than that at the interface of polymer-air ($\Delta N_{p,a}$ = 1.5-1.0 = 0.5). Similarly, the electric field and intensity distributions of TE1 mode are shown in Figure 5.3-(1) and 5.3-(2).

Figure 5.4 is the graphical solutions of TM modes for regular polymer (pure PMMA only). Two points can satisfy the eigenvalue equation, so TM0 and TM1 modes can exist in this regular waveguide. Figure 5.4-(1) and 5.4-(2) give the magnified curve from Figure 5.4, which can determine the eigenvalues of TM0 and TM1 modes individually. Since our detector mainly detect E-field intensity components, we plot the Ex component from which we get the intensity profile and compare it with the experimental results. Figure 5.5-(1) and 5.5-(2) show the unnormalized electric field and normalized intensity distributions for the TM0 mode. Figure 5.6-(1) and 5.6-(2) give the unnormalized electric field and normalized intensity profiles of TM1 mode.

From Figure 5.1-(1) and 5.1-(2) and Figure 5.4-(1) and 5.4-(2), eigenvalues of TE0, TE1, TM0 and TM1 (see the vertical label of graphs) can be obtained graphically:

TE mode, k_{x0} = 3.7102×10^5 m^{-1}; k_{x1} = 7.1548×10^5 m^{-1}.

TM mode, k_{x0} = 3.7338×10^5 m^{-1}; k_{x1} = 7.2206×10^5 m^{-1}.

The eigenvalues of TE0 and TM0, TE1 and TM1 are very close by comparing the eigenvalue difference (Δk_{x0} = 2.1×10^3 m^{-1}; Δk_{x1} = 6.58×10^3 m^{-1}), also it is very clear that the electric field and intensity profile match well for TE0 and TM0, TE1 and TM1 [see Figure 5.2-(1) & 5.2-(2) and 5.5-(1) & 5.5-(2), Figure 5.3-(1) & 5.3-(2) and 5.6-(1) & 5.6-(2)]. Both of the eigenvalues for TE0,1 smaller than

these for TMo,1.

Although the thickness of the metal for the structure APMPG (Air/Polymer/Metal/Polymer/Glass), is only 20 nm, the eigenvalues, the electric field and intensity profiles for both TE mode and TM mode have been totally changed. The reason is that the boundary conditions is totally different because of the thin metal film. Figure 5.7 and Figure 5.10 show the eigenvalues of TE mode and TM mode by using graphical method. Figure 5.7-(1) & 5.7-(2) and Figure 5.10-(1) & 5.10-(2) give the curves magnified from Figure 5.7 and 5.10. The eigenvalues of TEo,1 and TMo,1 are:

TE mode, $k_{xo} = 5.4769 \times 10^5$ m^{-1}; $k_{x1} = 6.7765 \times 10^5$ m^{-1}.

TM mode, $k_{xo} = 3.4161 \times 10^5$ m^{-1}; $k_{x1} = 7.1278 \times 10^5$ m^{-1}.

Now the eigenvalue difference of TEo and TMo, TE1 and TM1 are larger than that of PMMA only, the eigenvalue differences are $\Delta k_{xo} = 1.7667 \times 10^5$ m^{-1}, $\Delta k_{x1} = 3.783 \times 10^4$ m^{-1}, respectively.

The unnormalized electric field and normalized intensity profiles for TEo,1 and TMo,1 are shown in Figure 5.8-(1) & 5.8-(2) and 5.9-(1) & 5.9-(2), Figure 5.11-(1) & 5.11-(2) and 5.12-(1) & 5.12-(2).

By comparing Figure 5.2-(2) and 5.8-(2), Figure 5.3-(2) and 5.9-(2), Figure 5.5-(2) and 5.11-(2), Figure 5.6-(2) and 5.12-(2), it is very easy to get the conclusion: the modal distribution is effectively changed for every mode, especially for TE modes.

5.1.2 Experimental Results:

Figure 5-13 gives the intensity profiles of APMPG structure for
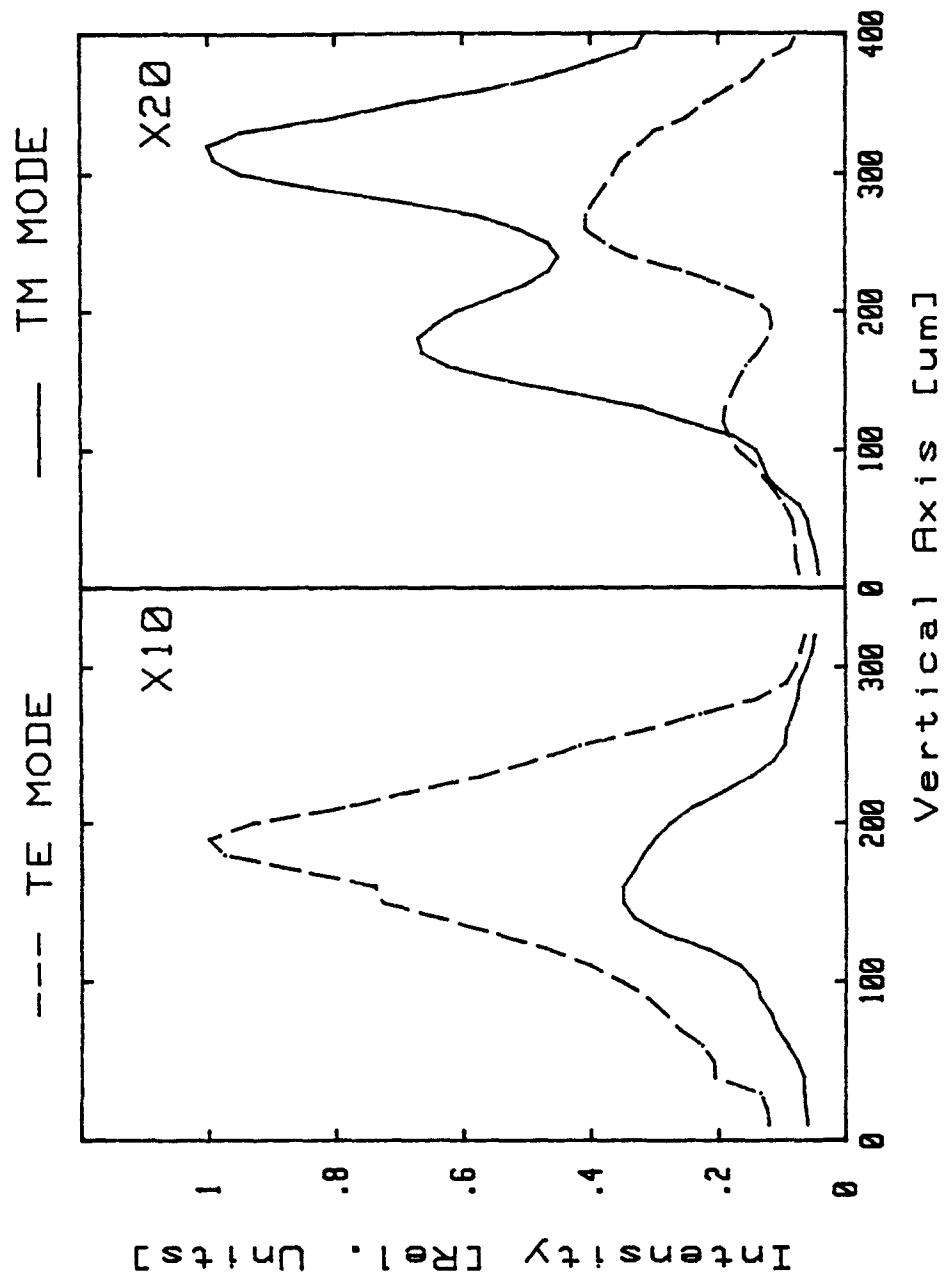
Figure 5.13   Intensity profiles of APMPG structure for

TE and TM mode using x10 and x20 lens.

both TE and TM modes using x10 and x20 objective lens. Alougth we cannot control the phase difference between TEo and TE1, TMo and TM1 modes, we can assume that the launching condition for TE and TM modes is fixed (during TE ↔ TM conversion, nothing is changed but turning the half-plate by 45^0). For x10 objective lens, the lower modes (such as TEo and TMo) are easily coupled to the waveguide because of the symmetric launching condition; for x20 objective lens, the relatively higher modes (such as TE1 and TM1) are easy to be coupled to the waveguide if the asymmetric launching conditions are maintained. We thus make the following conclusion: The TE mode which propagates in the waveguide is mostly symmetric and the TM mode of the waveguide is mostly asymmetric.

5.2 Intensity Profiles of Semiconductor Sandwiched Waveguides:

The measurement of a near-field intensity profile is a linear combination of the various modes,

$$ I = \left| E_0 + E_1 \cdot \exp(i\phi_1) + E_2 \cdot \exp(i\phi_2) + \cdots \right|^2 \qquad (5\text{-}1) $$

where E_1 is the mode amplitude and the ϕ_1 is the relative mode phase delay between the modes. In our case, we have only three TE modes, so the intensity can be represented by:

$$ I = \left| E_0 + E_1 \cdot \exp(i\phi_1) + E_2 \cdot \exp(i\phi_2) \right|^2 \qquad (5\text{-}2) $$

The near-field measurements for CdS sandwiched waveguides are shown in Figure 5. 14 and indicate the existence of three spatial TE

modes and two TM modes. Figure 5.14-(1) shows the TE modes with (the solid curve) and without (the dashed curve) illumination from a white light source. The TE modes tend to concentrate near the CdS film. Figure 5.14-(2) shows that no substantial effect is detected for the TM modes.
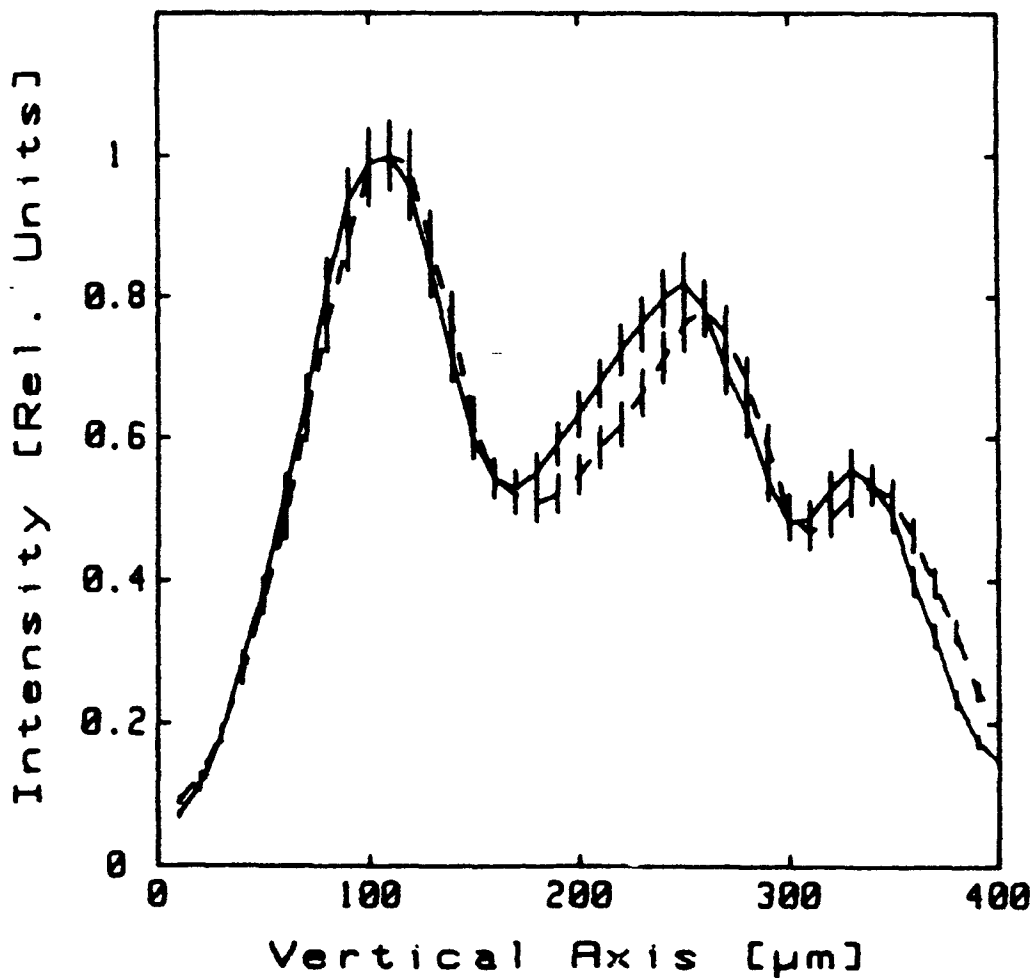
(1)
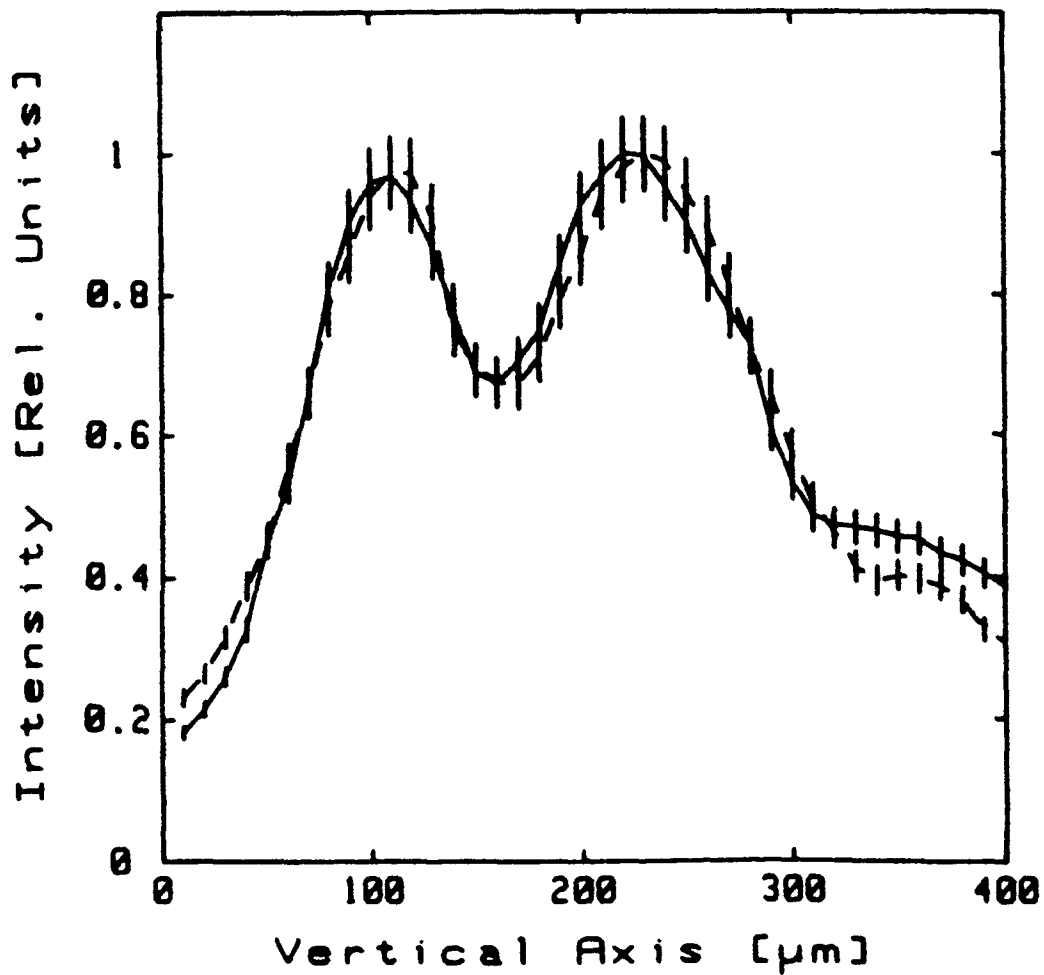
(2)

Figure 5.14 Intensity profiles for CdS layer embedded in a planar polymeric waveguide. (1) TE mode profile with illumination (the solid curve) and without illumination (the dashed curve). (2) TM mode profile with illumination (the solid curve) and without illumination (the dashed curve). The bars represent the exper- imental errors.

5.3 Waveguide scattering measurement:

We have studied guide loss as a function of guide length and temperature (here temperature factor is ignored and room temperature is assumed). Also included in these measurements are a study of various launch conditions and their effect on coupling loss.

A typical plot of scattered power distance resulting from this measurement technique is shown in Figure 5. 14. Analysis of this plot reveals that two slopes can be drawn through the data. The steeper slope in the first 2.5mm of the waveguide is attributed to coupling losses plus intrinsic losses. The coupling loss is due to launching conditions rather than waveguide characteristics. In this case, the light is launched into the waveguide through an optical lens. In this sample the combined loss value for TE mode is very large. The second slope occurs after the initial leaky modes have been stripped and is attributed to intrinsic waveguide losses. The intrinsic loss measured in this sample is 3.5 ± 0.1 dB/cm for TE mode and 3.2 ± 0.1 dB/cm for TM mode. The location of the scattering sites is obvious from the plot of the data. These data peaks, visually appear as bright, isotropically radiating points of light. Apart from causing the highly peaked spikes in the data, these sites can also cause instantaneous mode mixing within the waveguide.[18][19] After this occurs it requires some distance to recover. Over this distance, loss in the waveguide may vary as in the initial launch case. The last peak at the right is scattering from the waveguide output interface.
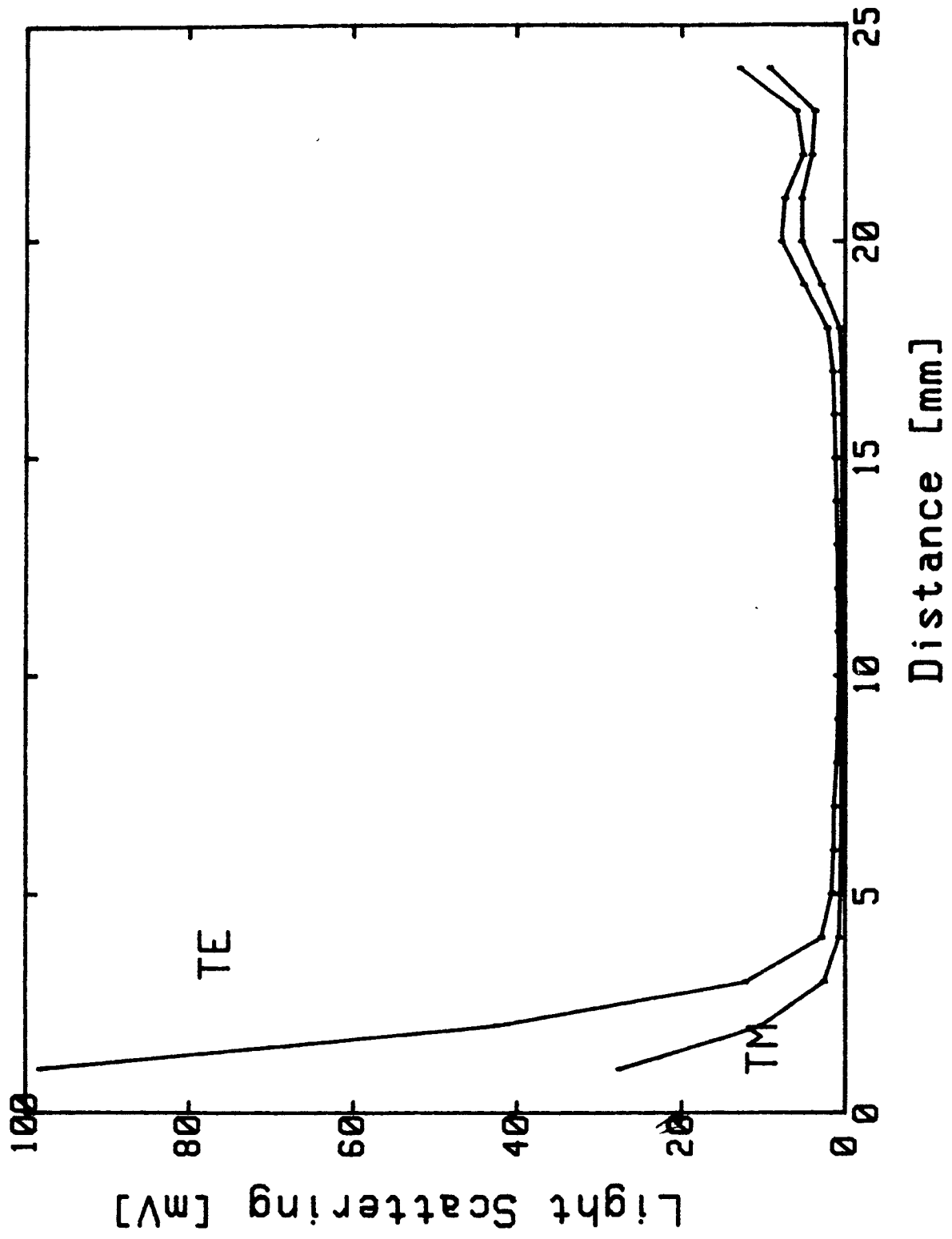
Figure 5.15   Scattering measurement of APMPG structure

waveguide.

CHAPTER 6   DISCUSSION

6.1   Comparison of Results from Theory and Experiments:

Comparing the theoretical figures (Figure 5.2-(2), 5.3-(2), 5.5-(2), 5.6-(2), 5.8-(2), 5.9-(2), 5.11-(2) and 5.12-(2)) and Figure 5.13 , for increasing Nartificial, the asymmetric TE mode is ''pushed'' to propagate outside the waveguide thus relatively less power is associated with the portion of the mode propagating inside the waveguide. We therefore expect that the asymmetric TE mode will be effectively suppressed due to the interaction with the radiation modes. For symmetric TE mode the field is mostly confined to the artificial layer region. For asymmetric TM mode the field distribution is mostly confined to the waveguide core region. For symmetric TM mode, it is mostly confined to the artificial layer region.

6.2   Discussions of Semiconductor Sandwiched Waveguides:

From Figure 5.14-(1) and 5.14-(2), the TE modes are much more sensitive to the external illumination than that of TM modes. This

phenomena can be explained as follows: The waveguide is homogeneously illuminated with light having a photo energy above the semiconductor band gap and that is capable of exciting the free carriers in the semiconductor clusters. These carriers effectively introduce a transverse interface for light propagating in the slab waveguide with a photo energy smaller than the semiconductor band gap. The short lifetime of the carriers will create mainly electric dipoles, i.e., an increase in the permittivity constant, while shielding currents are effectively suppressed owing to surface states, i.e., there is no change in the permeability constant. Continuity of the parallel electric field component at the cluster layer-polymer interface suggests that TE modes are more affected by the illumination than the TM modes.

CHAPTER 7 CONCLUSION

We established a waveguide fabrication system for which the generation rate is 330 Å/min, also we developed the method to fabricate artificial dielectrics (either metallic or semiconductor) multiple structure waveguides.

For the thin metallic sandwiched structure waveguides, the metallic layer in the waveguide center can play the role of a high dielectric constant material, it can effectively changes the modal distributions in the waveguide.[6] In the case of thin semiconductor layer, we show that the TE modes of a planar waveguide are more sensitive than the TM modes are to illumination of the semiconductor with light that creates excitations mainly of the electric dipoles. Owing to the presumably relatively short lifetime of the excited carriers, the magnetic dipoles are ineffective.

Potential applications for these kinds of waveguides may be found in the area of integrated optics. Control of the waveguide spatial mode distribution will be made by the introduction of active interfaces rather than by changes in the overall waveguide medium. Some of the advantages of these kinds of waveguides over the effective medium waveguides are that (1) the modes will propagate mainly in a linear medium and thus lead to smaller scattering losses, (2) changing

the waveguide boundaries requires relatively low power owing to the small volume involved, and (3) these waveguides are relatively easy to fabricate on a large class of substrates.[9][10]

REFERENCES

1. D. Marcuse, <u>Theory of Dielectric Optical Waveguides</u>, (Academic Press, 1974).

2. H. A. Haus, <u>Waves and Fields in Optoelectronics</u>, (Prentice-Hall, Inc., 1985).

3. A. W. Snyder and J. D. Love, <u>Optical Waveguide Theory</u>, (Chapman and Hall, 1983).

4. K. Iizuka, <u>Engineering Optics</u>, (2nd edition, Springer-Verlag, 1986)

5. M. Chien, <u>Transverse Electric (TE) and Transverse Magnetic (TM) Mode Conversion in Optically Active (Chiral) Embedded Polymeric Waveguides</u>, (M.S. Thesis, 1989).

6. I. P. Kaminow, W. L. Mammel and H. P. Weber, Applied Optics, Vol. 13, No. 2, 396-405 (1974).

7. J. D. Rancourt, <u>Optical Thin Films User's Handbook</u>, (McGraw-Hill, 1987)

8. D. L. Lee, <u>Electromagnetic Principles of Integrated Optics</u>, (John Wiley & Sons, Inc.,1986). Chapter 4 and Chapter 7.

9. H. Grebel and P. Chen, ''Artificial dielectric polymeric waveguides: metallic embedded films,'' has been accepted by Journal of Optical Society of America A.

10. H. Grebel and P. Chen, ''Artificial dielectric polymeric waveguides: semiconductor embedded films,'' Optics Letters,

Vol. 15, No. 12, 667-669 (June 15, 1990).

11. P. K. Tien, Applied Optics, Vol. 10, 2395 (1971).

12. R. Ulrich and R. J. Martin, Applied Optics, Vol. 10, 2077 (1971).

13. A. Yariv, Optical Electronics, 3rd Edition, (Holt, Rinehart and Winston, 1989). Chapter 12 and Chapter 13.

14. H. Kogelnik, Integrated Optics, (T. Tamir, ed., Springer, 1979). Chapter 2.

15. M. V. Klein, Optics, (Wiley, 1970). p.21.

16. P. K. Tien, G. Smolinsky and R. J. Martin, Applied Optics, Vol. 11, No. 3, 637-642 (1972).

17. D. H. Hartman, G. R. Lalk, J. W. Howse and R. R. Krchnavek, Applied Optics, Vol. 28, No. 1, 40-47 (1989).

18. N. Nourshargy, E. M. Starr, N. I. Fox and S. G. Jone, Electronics Letters, 21, 818 (1985).

19. K. Miura, I. Sawaki and H. Nakajima, in Technical Digest of Topical Meeting on Integrated and Guided Wave Optics, (Optical Society of American, Washington DC, 1988), pp. 58-61.

Appendix:

PROGRAM 1

```
C       PROGRAM 1 IS USED TO SOLVE THE EIGENVALUE
        EQUATION BY USING GRAPHICAL METHOD.
        DOUBLE PRECISION X, Y, AA, P, G, XA, XAT, XABT
        REAL*8 A, B, T, Np, NAl, Ng, N, K, PI
        PI = 3.1415926
        OPEN(1, FILE='CHENTE1.IN', STATUS='OLD')
        READ(1,3)X, STEP, XEND, A, B, T
        READ(1,3)Np, NAl, Ng, N
        CLOSE(1)
        K=2*PI/N
        OPEN(3, FILE='CHENTE1.OUT', STATUS='NEW')
1       X = X + STEP
        AA=(((Np*Np)-1)*K*K-X*X)**.5
        P=(((NAl*NAl)-(Np*Np))*K*K+X*X)**.5
        G=(((Np*Np)-(Ng*Ng))*K*K-X*X)**.5
        XA = 2.*PI*(X*A/(2.*PI)-INT(X*A/(2.*PI)))
        XAT = 2.*PI*(X*(A+T)/(2.*PI)-INT(X*(A+T)/(2.*PI)))
        XABT = 2.*PI*(X*(A+B+T)/(2.*PI)-INT(X*(A+B+T)/(2.*PI)))
        PA = 2.*PI*(P*A/(2.*PI)-INT(P*A/(2.*PI)))
        PAT = 2.*PI*(P*(A+T)/(2.*PI)-INT(P*(A+T)/(2.*PI)))
        IF (XA .EQ. 0.) GOTO 1
        IF (XAT .EQ. 0.) GOTO 1
        IF (XABT .EQ. 0.) GOTO 1
        IF (PA .EQ. 0.) GOTO 1
        IF (PAT .EQ. 0.) GOTO 1
        DEFB=TAN(XABT)-(AA/X)
        BB=1.0+(AA/X)*TAN(XABT)
        DEFC=-X*X*TAN(XA)+G*X+(x+G*TAN(XA))*P*TAN(PA)
        C=X*P+G*X*TAN(XA)-(G-X*TAN(XA))*X*TAN(PA)
        DEFW=-TAN((XAT))+DEFB/BB
        W=1.0+DEFB/BB*TAN(XAT)
        Y=DEFW/W
        Z=P*(-TAN(PAT)+DEFC/C)/(X*(1.+DEFC/C*TAN(PAT)))
        WRITE(*,2) X, Y, Z
        WRITE(3,2) X, Y, Z
        IF (X .GT. XEND) GOTO 4
        GOTO 1
2       FORMAT(' X = ',F15.7,' Y = ',F15.7,' Z= ' ,F15.7)
3       FORMAT(F20.10)
4       STOP
        END
```

PROGRAM 2

```
C      PROGRAM 2 IS USED TO GET ALL THE UNKONWN
       COEFFICIENTS.
       DOUBLE PRECISION X, Y, AA, P, G, Air
       REAL*8 A, B, T, Np, NAl, Ng, N, K, PI
       PI = 3.1415926
       A =4.0E-6
       B = 3.0E-6
       T = 6.E-8
       Np = 1.5
       NAl = 1.56
       Ng = 1.498
       X = 6.34030E5
       N=6.328E-7
       K=2*PI/N
       OPEN(3, FILE='PENG.OUT', STATUS='NEW')
       AA=(((Np*Np)-1)*K*K-X*X)**.5
       P=(((NAl*NAl)-(Np*Np))*K*K+X*X)**.5
       G=(((Np*Np)-(Ng*Ng))*K*K-X*X)**.5
       XA=X*A
       XAT=X*(A+T)
       XABT=X*(A+B+T)
       PA=P*A
       PAT=P*(A+T)
       PMMA3=1.
       PMMA4=PMMA3*(G/X)
       DEFC=-X*X*TAN(XA)+G*X+(X+G*TAN(XA))*P*TAN(PA)
       C=X*P+G*X*TAN(XA)-(G-X*TAN(XA))*X*TAN(PA)
       C1=DEFC/C
       Al1 = (COS(XA)+G/X*SIN(XA))/(COS(PA)+C1*SIN(PA))
       Al2=Al1*C1
       DEFB=TAN(XABT)-(AA/X)
       BB=1.0+(AA/X)*TAN(XABT)
       B1=DEFB/BB
       PMMA1=(Al1*COS(PAT)+Al2*SIN(PAT))/
     ! (COS(XAT)+B1*SIN(XAT))
       PMMA2=PMMA1*B1
       Air=(PMMA1*COS(XABT)+PMMA2*SIN(XABT))*
     ! EXP(AA*(A+B+T))
       WRITE(3,2)PMMA1, PMMA2, Al1, Al2, PMMA3, PMMA4, Air,
     ! AA, P, G
       WRITE(*,2)PMMA1, PMMA2, Al1, Al2, PMMA3, PMMA4, Air,
     ! AA, P, G
2      FORMAT(3(2X,D15.7))
4      STOP
       END
```

81

PROGRAM 3

```
C       PROGRAM 3 IS USED TO GET THE E-FIELD
        DISTRIBUTION.
        EY10(X)= -5.32958E-43*EXP(-X*1.106286E7)
        EY11(X)= 1.62316E-52*EXP(-X*1.107543E7)
        EY20(X)= .5507921*COS(X*9.213E5)+ 4.3466770*SIN(X*9.213E5)
        EY21(X)= 0.9398808*COS(X*7.544E5)+ 0.1525708*SIN(X*7.544E5)
        EY30(X)=-0.159365*COS(X*3.985421E6)-0.1234475*SIN(X*3.985421E6)
        EY31(X)=.4062652*COS(X*3.950364E6)+.0943032*SIN(X*3.950364E6)
        EY40(X)= COS(X*9.213E5)+ 0.210427*SIN(X*9.213E5)
        EY41(X)= COS(X*7.544E5)+ 0.1895423*SIN(X*7.544E5)
        EY50(X)= EXP(1.938709E5*X)
        EY51(X)= EXP(1.431803E5*X)
        X = -5E-6
        A = 5.5E-6
        B = 3.0E-6
        T = 2E-8
        OPEN(1,FILE='PENG2.OUT',STATUS='NEW')
C--------------------------
C   X LESS THAN 0
1       IF(X .GE. 0.) GOTO 2
                Y=(ABS(EY50(X)))**2.
                GOTO 6
C--------------------------
C   X GREAT THAN 0
2       IF(X .GE. A) GOTO 3
                Y=(ABS(EY40(X)))**2.
                GOTO 6
C--------------------------
C   X GREAT THAN A
3       IF(X .GE. A+T) GOTO 4
                Y=(ABS(EY30(X)))**2.
                GOTO 6
C--------------------------
C   X GREAT THAN A+T
4       IF(X .GE. A+B+T) GOTO 5
                Y=(ABS(EY20(X)))**2.
                GOTO 6
C--------------------------
C   X GREAT THAN A+B+T
5               Y=(ABS(EY10(X)))**2.
6       WRITE(1,7)X,Y
        WRITE(*,7)X,Y
        X = X + 1.E-7
        IF (X .GE. 9.5E-6) GOTO 8
        GOTO 1
7       FORMAT(' X = ',F15.11,'   Y = ',F15.7)
8       STOP
        END
```